Unclassified
Security Classification

AD 744 387

DOCUMENT CONTROL DATA - R & D

(Security classification of title, body of abstract and indexing annotation must be entered when the overall report is classified)

1. ORIGINATING ACTIVITY (Corporate author)
Air Force Institute of Technology (AFIT-EN)
Wright-Patterson AFB, Ohio 45433

2a. REPORT SECURITY CLASSIFICATION
Unclassified

2b. GROUP

3. REPORT TITLE
Zero-Phonon Line Absorption Spectra of Radiation Damage Centers in Silicon

4. DESCRIPTIVE NOTES (Type of report and inclusive dates)
AFIT Thesis

5. AUTHOR(S) (First name, middle initial, last name)
Kennedy B. Wilson
Capt. USAF

6. REPORT DATE	7a. TOTAL NO. OF PAGES	7b. NO. OF REFS
June 1972	94	41

8a. CONTRACT OR GRANT NO.	9a. ORIGINATOR'S REPORT NUMBER(S)
b. PROJECT NO. N/A	GNE/PH/72-11
c.	9b. OTHER REPORT NO(S) (Any other numbers that may be assigned this report)
d.	

10. DISTRIBUTION STATEMENT
Approved for public release; distribution unlimited.

11. SUPPLEMENTARY NOTES	12. SPONSORING MILITARY ACTIVITY
	AFIT-LPE W-PAFB, OH 45433

13. ABSTRACT

Infrared absorption measurements were made for n-type silicon samples irradiated with 1 MeV electrons at room temperature. The absorption spectra in the range 1-3 microns were recorded at both liquid nitrogen and liquid helium temperatures. Three families of zero-phonon lines and phonon-assisted sideband structure were seen which correspond to those seen in luminescence spectra. The families at 0.4891 eV and 0.7898 eV were seen only in pulled samples, while the family at 0.9702 eV was seen in both pulled and float-zone samples. A dose rate study indicated that all three families are independent of each other. The zero-phonon lines at 0.7898 eV, 0.7948 eV, and 0.9702 eV are independent of the divacancy. The growth rate of the line at 0.4891 eV may follow that of the divacancy. The splitting of the zero-phonon line at 0.7898 eV occurs in the excited state since both the zero-phonon lines at 0.7898 eV and 0.7948 eV occurred at equal intensity in the low temperature absorption spectra. (U)

I

DD FORM 1 NOV 65 1473

Unclassified
Security Classification

Unclassified
Security Classification

KEY WORDS	LINK A		LINK B		LINK C	
	ROLE	WT	ROLE	WT	ROLE	WT
Semiconductors						
Radiation Damage in Silicon						
Absorption Spectra						
Electron Irradiation						
Dose Rate Study						
Zero-Phonon Lines						

Ia

ZERO-PHONON LINE ABSORPTION SPECTRA OF RADIATION DAMAGE CENTERS IN SILICON

THESIS

GNE/PH/72-11 Kennedy B. Wilson
Captain USAF

Approved for public release; distribution unlimited.

GNE/PH/72-11

ZERO-PHONON LINE ABSORPTION SPECTRA OF RADIATION DAMAGE CENTERS IN SILICON

THESIS

Presented to the Faculty of the School of Engineering of
the Air Force Institute of Technology
Air University
in Partial Fulfillment of the
Requirements for the Degree of
Master of Science

by

Kennedy B. Wilson, B.A.C.
Captain USAF

Graduate Nuclear Engineering
June 1972

Ic

Preface

This report is the result of my efforts to study the nature of radiation defects in a semiconductor material. I accepted a proposal, from the Air Force Materials Laboratory, to record absorption spectra from irradiated silicon samples and to correlate the results with those found by recombination luminescence. The correlation of these results with luminescence spectra indicate the usefulness of absorption techniques in studying radiation damage in silicon.

I would like to thank Dr. Jon Meese at the Solid State Physics branch of the Aerospace Research Laboratory for providing access to the Van de Graaff generator for irradiation of the samples used in this study. I am grateful to Mr. Jacque D. Henes of the University of Dayton Research Institute for his assistance in certain phases of the experimental program.

I would also like to thank Lt. Col. John S. DeWitt for his interest in this project.

I owe a special debt of gratitude to Dr. Robert J. Spry of the Air Force Materials Laboratory for his guidance and involvement in this thesis project. His informative discussions aided me greatly in the performance of this project.

KBW

Contents

Contents

List of Figures

List of Tables

Abstract

Infrared absorption measurements were made for n-type silicon samples irradiated with 1 MeV electrons at room temperature. The absorption spectra in the range 1-3 microns were recorded at both liquid nitrogen and liquid helium temperatures. Three families of zero-phonon lines and phonon-assisted sideband structure were seen which correspond to those seen in luminescence spectra. The families at 0.4891 eV and 0.7898 eV were seen only in pulled samples, while the family at 0.9702 eV was seen in both pulled and float zone samples. A dose rate study indicated that all three families are independent of each other. The zero-phonon lines at 0.7898 eV, 0.7948 eV, and 0.9702 eV are independent of the divacancy. The growth rate of the line at 0.4891 eV may follow that of the divacancy. The splitting of the zero-phonon line at 0.7898 eV occurs in the excited state since both the zero-phonon lines at 0.7898 eV and 0.7948 eV occurred at equal intensity in the low temperature absorption spectra.

ZERO-PHONON LINE ABSORPTION SPECTRA OF RADIATION DAMAGE CENTERS IN SILICON

I. Introduction

Silicon is the ... oup IV element with an atomic number of 14 lying above carbon and below germanium in the periodic table. Electrically, it is classified as a semiconductor. In its purest form silicon has a room temperature resistivity of approximately 2.5×10^5 ohm-cm. The addition of 5×10^{15} atoms/cm^3 or about 1 part per 10 million of an impurity can bring the room temperature resistivity down to 10 ohm-cm. This characteristic of having the carrier concentration determined by the impurities makes silicon an important electrical material. Silicon, with controlled impurity concentrations, is used in diodes, transistors, integrated miniature circuits, and many more components of the rapidly increasing solid state electronics field.

Just as chemically added impurities affect silicons electrical properties, lattice defects produced by radiation can also affect these properties. Because of the increasing need to use silicon devices in space, and in military equipment, there has been an extensive program to investigate radiation effects in silicon. Much effort has been devoted to understanding the mechanisms of developing defect formation, identifying various defect

models, and developing some radiation hardening methods.

Since most of the radiation induced defects in semiconductors are on the atomic scale, there is no direct method which can furnish all the information needed to describe the defects. Instead, indirect methods, through various defect sensitive physical properties of the material, are employed. By the interpretation and correlation of a number of experiments on different properties, a consistent model may be obtained of the configuration of defects as they exist in the crystal.

One useful technique which can reveal information on the microscopic nature of defects is recombination luminescence. A study of defect luminescence spectra can give information on the defects' energy levels in the gap, the nature of the recombination processes, and the interaction of defects with the lattice. Low temperature photoluminescence has been used by Yukhnevich and Tkachev (Ref 41) in the Soviet Union, and by Spry and Compton (Ref 33), Jones and Compton (Ref 22), and Johnson and Compton (Ref 20) in the United States to study those defects. The spectra consist of strong zero-phonon lines accompanied by phonon-emission bands on the low energy side of the zero-phonon lines.

Another technique which can give information of the microscopic nature of defects is optical absorption. Recently, Bean, et al. (Ref 4) have reported detecting several new absorption bands at liquid nitrogen temperature in electron irradiated silicon which are thought to be of

electronic origin. These bands occurred at energies which correspond to zero-phonon line energies seen in photoluminescence spectra. Dean, et al. (Ref 13) identified zero-phonon components in absorption spectra due to bound excitons in silicon by comparing the transition energies in the absorption and luminescence spectra.

The purpose of the project described in this thesis was to obtain liquid nitrogen and liquid helium temperature absorption spectra from electron irradiated silicon samples which showed the same narrow lines reported by Bean, et al. A search was to be made for other narrow lines which occurred in luminescence spectra and a correlation made between the absorption and luminescence bands. A high resolution recording spectrophotometer was used to record absorption spectra at both liquid nitrogen and liquid helium temperatures.

After the initial absorption spectra recorded indicated the existence of these new absorption bands, a growth rate study of the prominent bands was undertaken. The intensity of the bands was studied as a function of the electron fluence in an attempt to identify the defects responsible for the spectra.

The next three chapters that follow contain the background information pertinent to this study of silicon. The information presented include the general properties of silicon, the optical properties of silicon, and a discussion of electron radiation damage in silicon. The final three

chapters discuss equipment and procedures, experimental results, and discussion and conclusions.

II. General Properties of Silicon

This section contains information on the growth methods, band structure, and phonon spectrum of single crystals of silicon. The crystal growth methods are discussed because they can give valuable information concerning chemical impurities in silicon. Both the electronic energy band structure and the lattice vibronic structure are extremely important in determining the optical properties of silicon.

Crystal Growth

The concentration and type of chemical impurity in silicon are determined by the method of crystal growth. Large single crystals of silicon are most often produced by the Czochralski method. In this method, a seed crystal is dipped into the melt and then drawn from the melt by a rod which can be simultaneously rotated and raised. The molten silicon is normally contained in a quartz crucible. At the melting point of silicon, 1420°C, oxygen is readily exchanged between the crucible and the molten silicon. Crystals produced by this method contain oxygen in interstitial positions in concentrations of nearly 10^{18} per cm^3 (Ref 23:812).

The other common method for producing single crystals of silicon is by the float zone technique. In this technique, a radio frequency coil is passed along the length of a vertically held silicon rod. A thin molten zone is produced by the heating coil and is swept through the crystal. Very pure crystals are produced by this method

since the impurities have a higher solubility in the melt than in the solid and are segregated at the bottom. The oxygen concentration is approximately 10^{16} per cm^3 (Ref 23:882).

Residual impurities, other than the intended dopant, which are of interest in radiation damage are oxygen, carbon, and germanium. Bean, et al. (Ref 4:751) reported a carbon content of $2x10^{18}$ per cm^3 in a pulled crystal not deliberately doped with this impurity. Baker, et al. (Ref 3:4368) found the carbon concentration in float zone silicon to be on the order of 10^{17} per cm^3.

Band Structure

As silicon atoms are brought together to form a crystal, energy bands are formed at an equilibrium lattice spacing. The corresponding crystal structure for silicon as a function of wave vector $\vec{k}$ is shown in Fig. 1.

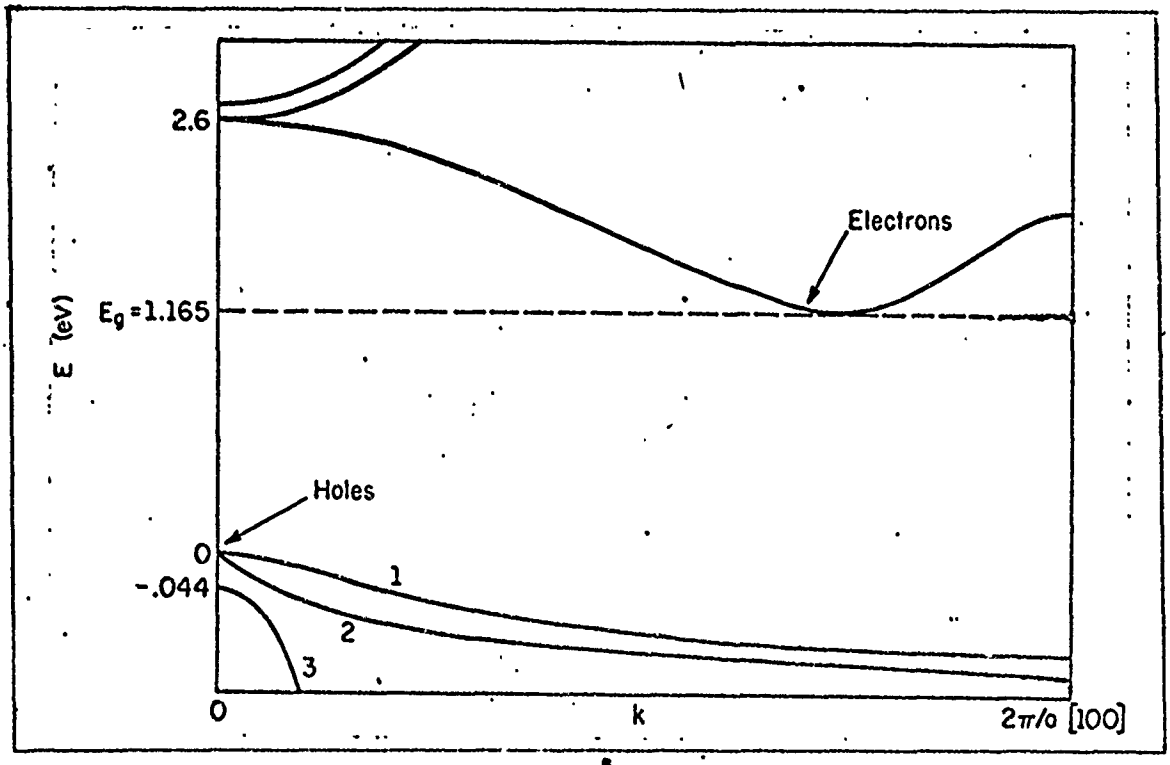

Fig. 1. Energy Band Structure of Silicon (Ref 21)

The valence band maximum occurs at $\vec{k}=0$, the center of the first Brillouin zone. However, the conduction band minimum occurs at approximately 82% of the distance toward the direction of the first Brillouin zone boundary. For this reason silicon is termed an indirect band gap semiconductor. The indirect band gap energy is 1.165 eV at liquid helium temperature (Ref 32:352).

Phonon Spectrum

As a result of the difference in energy between the indirect gap and the direct gap in silicon, most conduction band electrons occupy states near the conduction band minimum. It is these electrons which dominate the electrical and optical properties of the material. In order to conserve crystal momentum, electronic transitions occur with phonon assistance. The phonon spectrum of silicon for the case of lattice vibrations propagating in the [100] direction in silicon at room temperature is shown in Fig. 2. The spectrum for silicon exhibits both the optical branch and the acoustic branch. Each of these branches has two different modes of vibrations with the displacement of atoms either transverse or longitudinal to the direction of wave propagation. The $\vec{k}$ value corresponding to the minimum in the conduction band is shown by the dotted line. The energies of the phonons having the appropriate momentum to make the indirect transition possible are equal to 0.059 eV, 0.053 eV, 0.044 eV, and 0.018 eV. The phonons with largest densities of states at this point are the TO phonon at 0.059 eV, the TA phonon at 0.018 eV, and the zone center optical phonon at 0.064 eV.

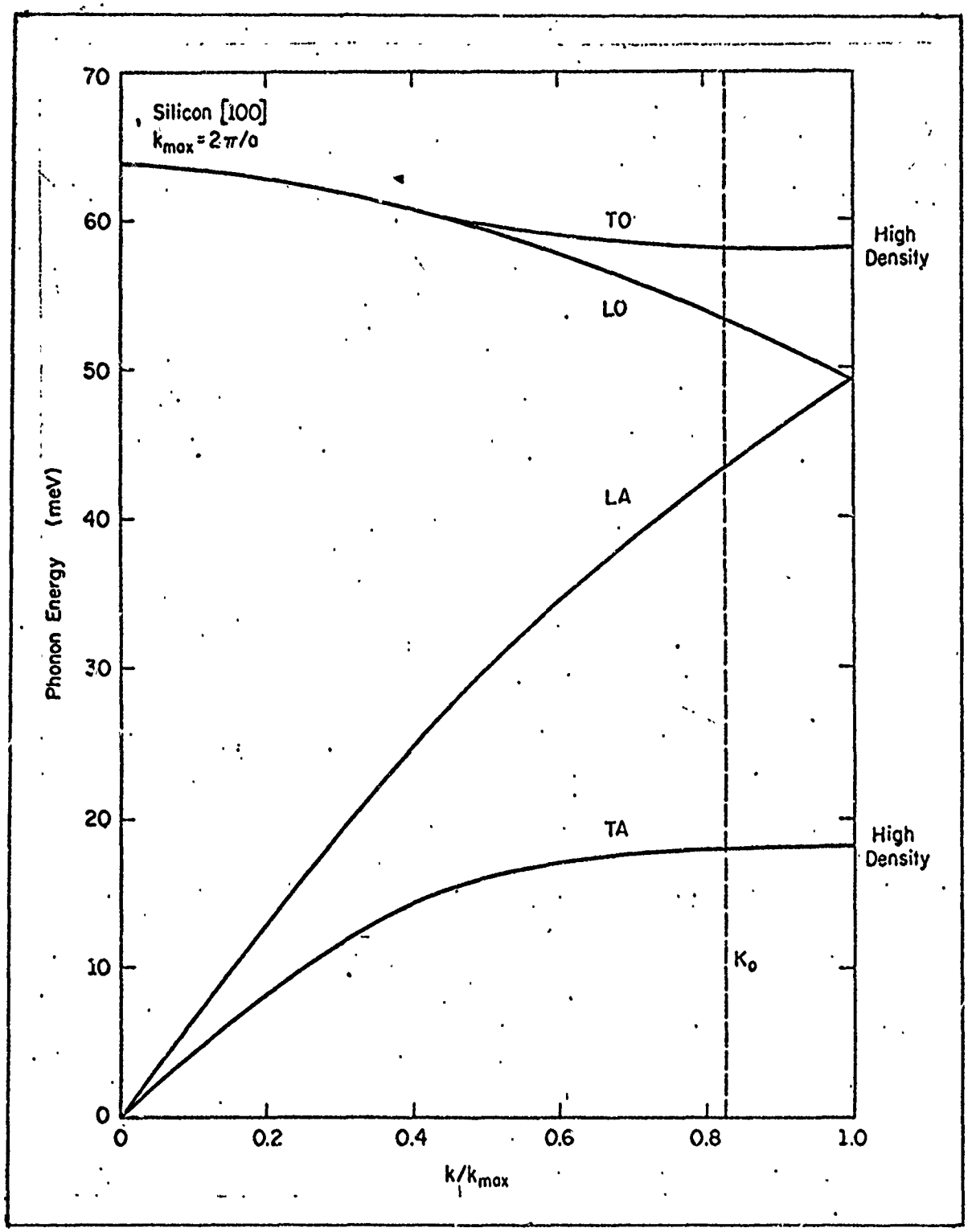

Fig. 2. Phonon Spectrum of Silicon (Ref 7 :256)

III. Optical Properties

The first section of this chapter contains information on the absorption of electromagnetic radiation in silicon. The next two sections include background material on free excitons and bound exciton absorption. Zero-phonon transitions are then discussed with the resulting spectra identified as an optical analog of the Mössbauer effect.

Absorption Process

Fundamental absorption takes place when an electron is excited by the absorption of a photon. There are two types of transitions which can occur. Transitions in which only a photon is involved are referred to as direct. Those in which energy is either supplied by the crystal lattice or given up to it, are referred to as indirect. In this type, one or more phonons are emitted or absorbed at the same time as the photon is absorbed. As was shown in Fig. 1, the lowest energy state in the conduction band of silicon does not have the same value of $\vec{k}$ as the highest energy state in the valence band. Direct transitions will only be possible with visible photons and any infra-red absorption must arise from indirect transitions (Ref 27 :114).

For the indirect transition to take place in an absorption process, crystal momentum must be conserved. The amount of momentum needed is supplied by either the absorption or emission of a phonon. The direct transition is labeled D and the indirect transition is labeled I in Fig. 3.

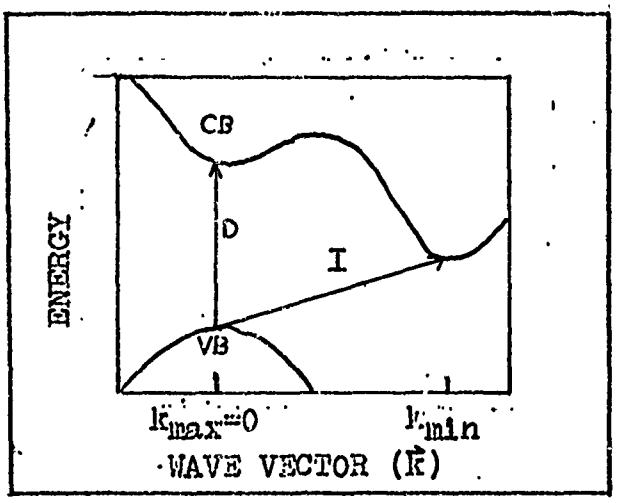

Fig. 3. Band-to-Band Transitions

The photon energy required for transition I is given by

$$h\nu = E_g \pm \hbar\omega \tag{1}$$

where E_g is the energy gap and $\hbar\omega$ is the energy of the phonon. The $\pm$ refers to the emission and absorption of the phonon, respectively. At low temperatures, the density of phonons in the crystal will be so small that phonon absorption is negligible (Ref 26:1245).

In absorption spectra, the absorption coefficient is usually plotted as a function of photon energy. The absorption coefficient can be defined as the product of the cross section for absorption and the volume density of absorbing atoms. When the photon has energy enough to excite electrons from the valence band to the conduction band, a large

increase in absorption is observed (Ref 32:191). The absorption coefficient for silicon, as shown in Fig. 4, indicates the increase in absorption as the photon energy increases.

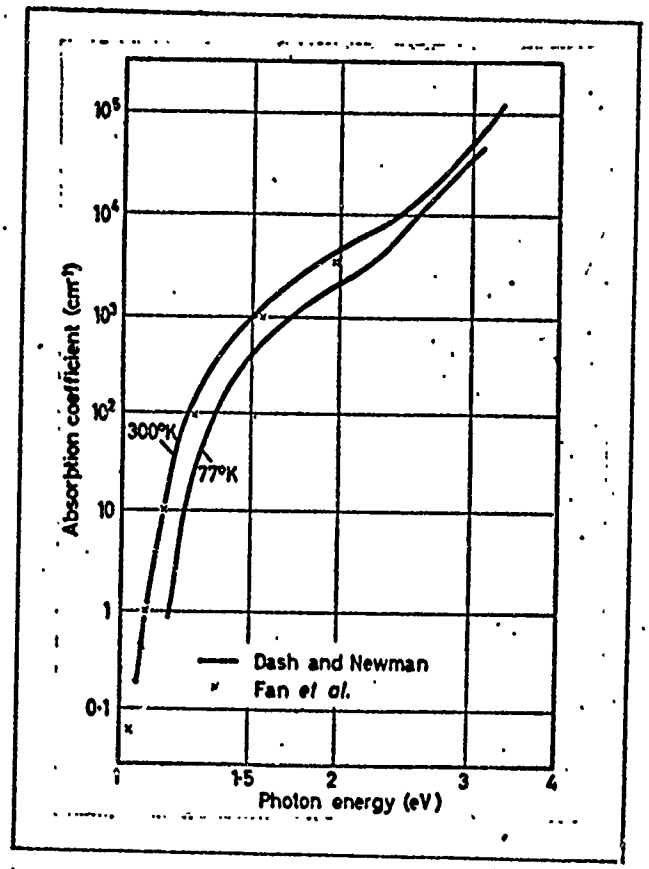

Fig. 4. Absorption in Silicon (Ref 27:116)

The figure can be interpreted as showing the onset of indirect transitions at approximately 1.1 eV at room temperature.

So far the discussion has only concerned band-to-band absorption, which by definition generates a free hole and free electron. However, if the energy of the photon is not sufficient to excite an electron from the valence band to

the conduction band, various optical transitions from impurity centers may be induced within a band. These impurity centers may result from the substitution of a group III atom (acceptor) or a group V atom (donor) into the crystal lattice. The energy levels of the donor and acceptor lie very near the conduction and valence bands. Since these energies are so near to the conduction or valence bands, it is necessary to cool to very low temperatures before the density of impurity centers which are unionized is sufficient to give significant absorption (Ref 27:50). If silicon is heavily doped with both donors and acceptors, absorption may be due to donor-acceptor pair formation. The model for this transition is an electron bound to an unionized donor and a hole bound to an unionized acceptor. The energy of the absorption process is given by

$$h\nu = E_g - (E_D + E_A) + \sum_i \hbar\omega_i + \frac{e^2}{\epsilon r} \qquad (2)$$

where E_D and E_A are the ionization energies of the donor and acceptor, $\hbar\omega$ is the energy of a momentum conserving phonon, e is the charge of an electron, ϵ is the static dielectric constant, and r is the separation between donor and acceptor. The absorption peak will be narrow with no thermal broadening of the halfwidth, but may be broadened by the $\frac{e^2}{\epsilon r}$ term.

The effect of high energy particle irradiation also produces defect centers in the crystal lattice. The defect may act as a donor or acceptor site (Ref 14:1127).

Information on the defect's energy level may be obtained by measuring the infrared absorption beyond the fundamental band edge (Ref 35:169).

Excitons

Because an electron and hole have an attractive Coulomb interaction, it is possible for stable bound states of the two particles to be formed. This bound electron-hole pair known as an exciton, is a neutral, excited state of a crystal.

There are two different limiting approximations for the exciton concept. The Frenkel exciton is considered as a tightly bound pair whereas the Wannier exciton is a weakly bound pair (Ref 25). The Wannier exciton structure is analogous to the hydrogen atom model. The ground state ionization energy G, is calculated from

$$G = \frac{13.6\mu}{\epsilon m_o} \tag{3}$$

where μ is the reduced mass of the electron-hole pair and m_o is the free electron mass.

The excitation energy necessary for the creation of a free exciton at low temperatures, a characteristic of the band structure of a pure material, is given by

$$h\nu = E_g - G + \sum_i \hbar\omega_i + (E_T)ex \tag{4}$$

where $(E_T)ex$ is the translational thermal energy of the exciton. In both equations (2) and (4) $\sum_i \hbar\omega_i$ may be zero.

Bound Exciton Absorption

The first experimental proof of bound excitons was shown by Haynes (Ref16). He observed sharp lines close to the exciton energy gap in low temperature luminescence spectra of silicon. The luminescence was due to the radiative decay of excitons bound to a variety of neutral donor and acceptor centers. Dean, et al. (Ref13) reported weak, but sharp, absorption bands due to the creation of excitons bound to neutral donor and acceptor centers in silicon. The spectrum, shown in Fig. 5, included a zero-phonon component and two momentum conserving phonon-assisted component. A splitting was observed for the acceptor-exciton complexes,

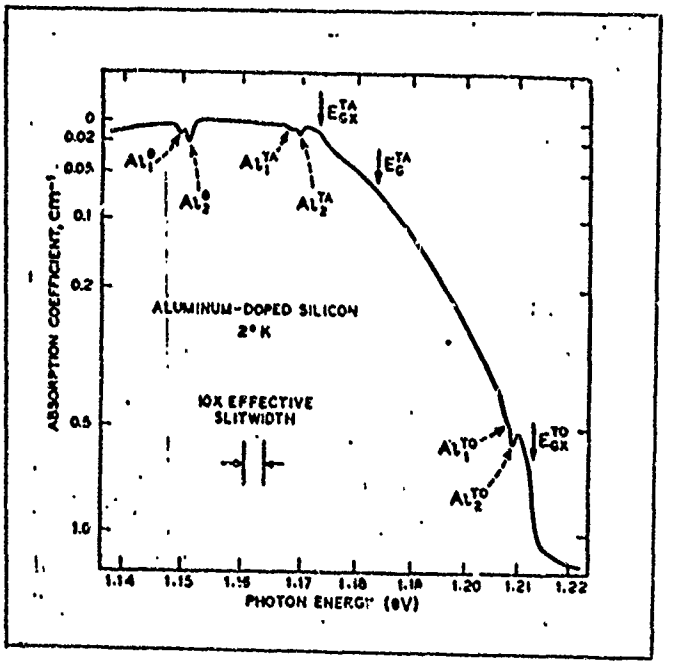

Fig. 5. Bound Exciton-Acceptor Spectrum (Ref 13:722) Splitting is shown by subscripts 1 and 2.

as is shown in Fig. 5. The magnitude of this splitting was found to be proportional to the localization energy of the bound exciton and therefore to the ionization energy of the acceptor.

The energy required for the creation of a bound exciton is given by

$$h\nu = (E_g - G) - E_L + \sum_i \hbar\omega_i \qquad (5)$$

where E_L is the localization energy binding an exciton to a center. Haynes found (Ref16 :362) that, to a good approximation, the energy for an exciton bound to a neutral Coulombic center is

$$E_L = 0.1\ E_I \qquad (6)$$

where E_I is the ionization energy for a single carrier trapped at the defect.

Excitons may also be bound to ionized donor or acceptor impurities. In this case the localization energy is given by

$$E_L \cong E_I \qquad (7)$$

However, theoretical work has suggested that excitons bound to ionized donor or acceptor impurities are not stable in silicon (Ref17 :726).

Zero-Phonon Spectra

Spectra of many crystals at low temperatures consist of narrow absorption and emission lines. The narrow lines are characterized by zero-phonon lines accompanied by

several phonon-assisted sidebands. The sidebands arise during the emission or absorption of a photon and the simultaneous excitation of phonons. A zero-phonon line can often be recognized as such by its extreme narrowness, and can usually be proved to be such by the observation of an emission and absorption line at the same frequency (Ref 34:242). The phonon assisted sidebands formed in absorption and emission spectra often have mirror symmetry about the zero-phonon line. In Fig. 6, a comparison of the emission and absorption spectra of diamond exhibit this mirror symmetry.

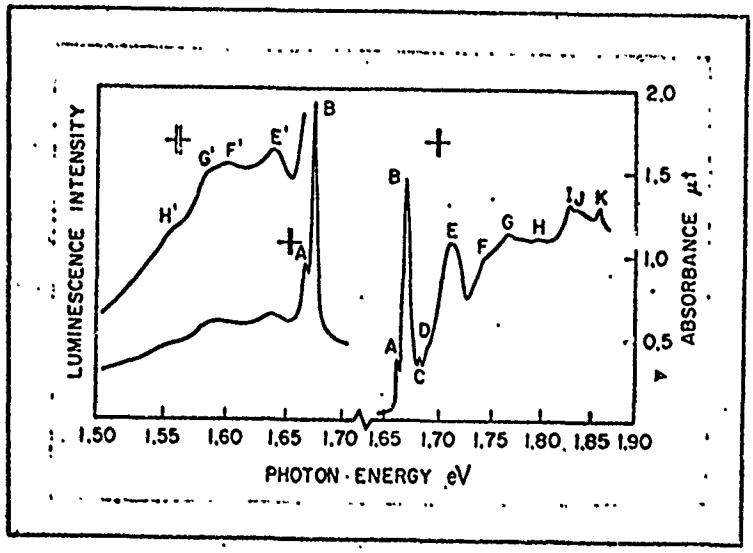

Fig. 6. Emission and Absorption Spectra of Electron Irradiated Type IIa Natural Diamond (Ref 39:188) Mirror symmetry about zero-phonon line B.

Zero-phonon lines occur in the optical spectra of defects in solids in much the same way that narrow, recoil-free Mössbauer lines appear in the gamma ray spectra of solids (Ref 15:294). For the optical case, the photon supplies energy to the crystal for the electronic

transition. There is a displacement recoil associated with this transition as the neighboring atoms relax to new equilibrium positions. The displacement recoil involves the excitation of several vibrational modes of the crystal or phonons which shift and broaden the absorption peak. The states of excitation are quantized so there is a finite probability that no mode will be excited. This is the case resulting in a zero-phonon line that is neither displaced nor broadened by energy transfered to the lattice modes.

The absorption spectrum will consist of a series of lines at

$$E_i = E_o + \hbar\omega_i \tag{8}$$

where E_o is the zero-phonon transition energy and i designates the phonon branch (TA, TO, etc.). For the emission spectrum the series of lines is given by

$$E_i = E_o - \hbar\omega_i \tag{9}$$

If an exciton is weakly bound to a defect, then phonon-assisted transitions must predominate (Ref12 :190). The phonons involved will be the TA and TO phonons seen in the intrinsic absorption edge. At an intermediate amount of exciton-center coupling, the relative intensity of the zero-phonon line will increase. When the exciton becomes tightly bound, phonon-assisted transitions again predominate. The phonon-assisted sideband structure may then contain

a series of evenly spaced peaks corresponding to electronic transitions in which one, two, or more phonons are simultaneously emitted (Ref 12:190). For silicon multiples of the TA phonon would be expected (Ref 21:180).

IV. Electron Radiation Damage in Silicon

Discussed in this section are the defect production mechanisms, the methods for studying these defects, and some of the known defects in silicon.

Defect Production

Defects in the perfect silicon crystal lattice include the chemical impurites such as group III or group V dopants, oxygen, and carbon, and the structural imperfections created during the crystal growth process. Other point defects such as vacancies and interstitials can be induced in the crystal by the bombardment with high energy particles. If the energy of the particle is high enough, Frenkel defects or more complex defects such as the divacancy may be formed. Since the simple radiation damage defects such as vacancies are mobile, even at low temperatures, more complicated defect structures result. These complexes are formed with the other structural imperfections and chemical impurities. This complexing of defects complicates the investigation of the defect structure of the crystal.

The high energy particles such as electrons and neutrons collide with the lattice and transfer energy to the lattice. If this energy is greater than the displacement energy, E_d, atoms are displaced.

In electron irradiation, the damage is caused by electron-nuclei scattering due to Coulomb interaction. The maximum energy that can be transferred to a lattice

atom by a relativistic electron is

$$E_{Amax} = 2E_e (E_e + 2m_o c^2)/Mc^2 \qquad (10)$$

where E_e and m_o are the energy and rest mass of the electron, M is the mass of the struck atom, and c is the speed of light. The maximum energy that can be transferred to a silicon atom by 1 MeV electrons is 155 eV. Cahn (Ref 8 :1311) calculated the average number of displaced atoms per 1 MeV electrons to be less than 1 for an E_d of 30 eV. The damage produced by electron irradiation is not uniform unless very thin samples are used. To overcome this disadvantage, the samples used in this study were irradiated to equal fluences on both sides. A damage profile will be given in the next section.

Methods of Defect Study

As mentioned before, there is no one technique capable of providing all the necessary information about a defect. It is necessary to take data from several types of measurements to obtain a complete picture of the radiation damage process. Each of the different techniques has its own advantages and disadvantages, and thus its own region of application. Techniques such as photoconductivity, electron spin resonance, luminescence, and optical absorption have been used for studying defects in irradiated silicon.

In photoconductivity studies, the conductivity of the sample is measured as it is illuminated with monochromatic light. As the photon energy varies, steps in the conduc-

tivity occur which correspond to the onset of transitions into the valence or conduction band. The photon energy for which the step occurs gives the energy of the defect level measured from a band edge. Photoconductivity measurements therefore can only give information on electronic transitions to a band and are of no value in studying electronic transitions between bound energy states.

In the absorption technique, the photon energy of the incident light can cause electronic transitions to excited states of a defect, electron transitions to a band edge, and the excitation of the local modes of the defect. This technique requires that the concentration of the defects be on the order of 10^{14} per cm^3 to 10^{18} per cm^3 (Ref 10:45) for electronic transitions. Transitions to and from the ground state of the defect are dependent on the position of the Fermi level. The Fermi level must lie below the ground state in order to observe transitions from the valence band into the ground state. Transitions out of the ground state into the conduction band or into higher excited states requires the Fermi level to be above the ground state. Information on determining which bands belong to the same defect and the identification of the defect may be accomplished by two methods. One method is to study the annealing behavior of the absorption bands. The other is to measure the intensity of the bands as a function of radiation dose or impurity concentration. Additional information may be obtained by applying uniaxial stress to

the sample while illuminating it with polarized light and measuring the change in absorption.

To identify radiation defects, electron spin resonance has been the most useful tool. In this technique, the interaction between the electronic magnetic moments and a static magnetic field is studied. Resonance patterns occur as a function of the crystallographic orientation relative to the static magnetic field. The symmetry of the defect structure can be deduced from these patterns. The defect's energy levels are estimated by observing the change in the resonance patterns while the Fermi level is passed through the defect level.

Recombination luminescence is limited to the study of defects in which a trapped carrier recombines through a radiative process, as opposed to a non radiative process. Radiative transitions occur either through band-to-band recombination or through the defect energy levels.

Known Defects in Irradiated Silicon

The primary defects produced by high energy radiation in silicon are vacancies and interstitials. However, the vacancy and interstitial are mobile at very low temperatures and can move through the crystal to form more complicated defect structures. These include the divacancy and the impurity-vacancy complex.

When a lattice vacancy is formed by the radiation damage event, an interstitial must also be formed. However, there has been no direct evidence for the isolated interstitial atom. Watkins (Ref 36:72) has suggested that

the interstitial is mobile even at 4.2°K and has presented a model to account for the disappearance of the isolated silicon interstitial.

The isolated vacancy has been observed by Watkins (Ref 36:68) using the electron spin resonance technique. Since the vacancy is mobile at low temperatures, it can join with impurity atoms to form impurity-vacancy complexes such as the A center and E center.

The A center is a vacancy-oxygen complex (Ref 10:75). When the vacancy is trapped by oxygen, the previously interstitial oxygen fills the vacancy site and thereby becomes substitutional. This center has been found in both pulled and float zone irradiated silicon (Ref5,11,38). The A center concentration increases with integrated bombarding flux, as long as there remains sufficient interstitial oxygen with which the vacancy may combine.

The E center is a vacancy-phosphorus complex and found mainly in float zone material (Ref 37). In this case the vacancy is trapped next to the substitutional phosphorus and the vacancy site is not filled.

The divacancy is produced either directly in the radiation damage event or indirectly by a combination of two mobile vacancies. Formation of the divancancy is enhanced by the presence of oxygen and carbon (Ref 4 :745).

Other defects have been detected for which there are no firmly established structural models. Such a defect, the K center, is found only in pulled silicon and is thus

assumed to be dependent on oxygen for its formation (Ref 1).

Previous Results

This section contains the previously reported results from absorption and luminescence spectra which occur in the spectral range examined in this project One absorption spectrum and two luminescence spectra are shown. A table is included containing reported values with which to compare the results obtained in this study.

Absorption Studies. Bean, et al. (Ref 4) reported a sharp line absorption spectrum of two, high resistivity, p-type pulled silicon samples irradiated with $5x10^{18}$ e/cm^2. The spectrum was recorded at liquid nitrogen temperature using the differential technique. This technique employed the use of two samples of the same thickness. One sample, which had been irradiated, was mounted in a liquid nitrogen dewar and placed in the sample compartment of a double beam grating Grubb Parsons Spectromaster (Ref 29:1495). An unirradiated sample of high purity prepared by the float zone technique was mounted in another liquid nitrogen dewar and placed in the reference compartment. For this spectrometer arrangement, white light falls on the samples (Ref 4:741). In the differential technique the intrinsic absorption is completely eliminated from the recorded spectrum. The spectrum of two different samples, of varying carbon content is shown in Fig. 7.

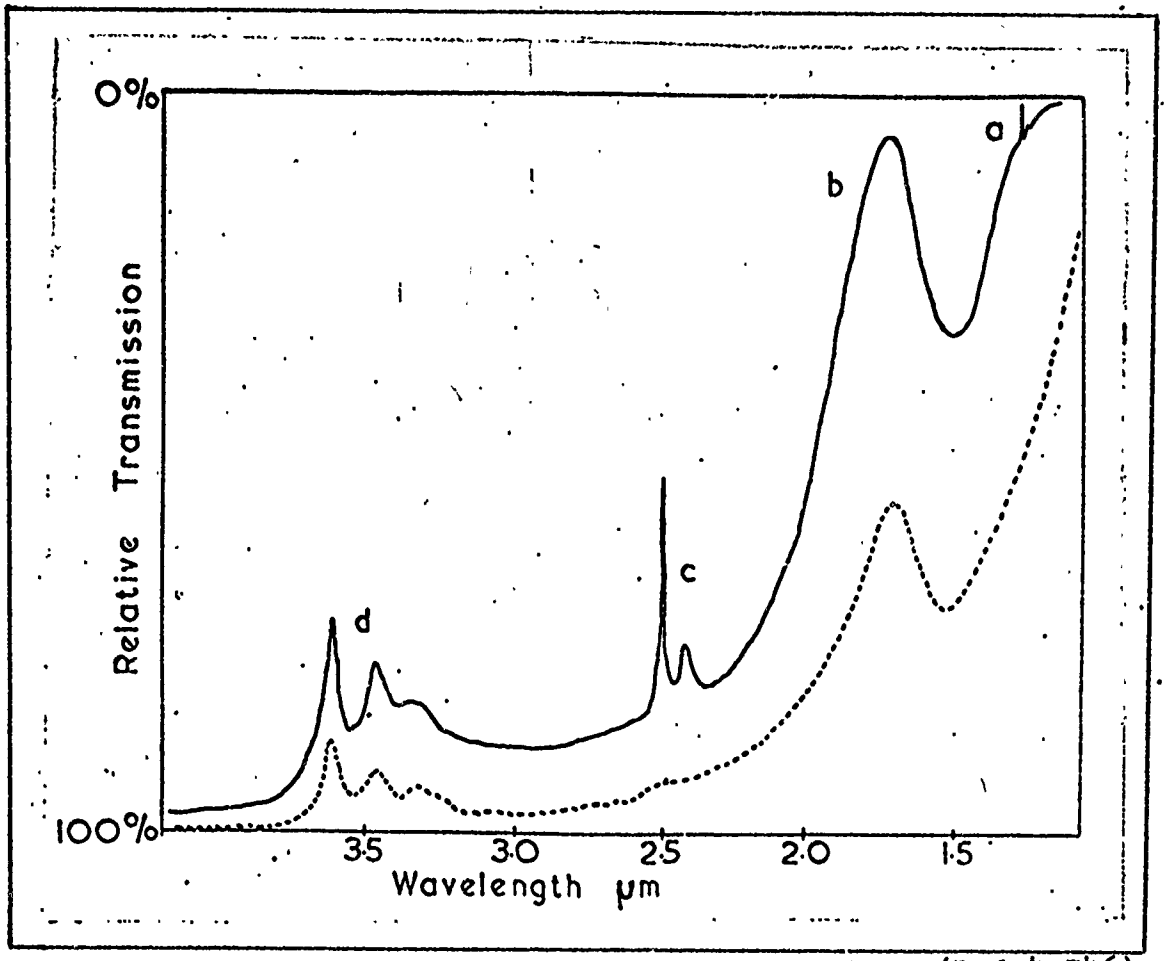

Fig. 7. Relative Transmission of Irradiated Silicon (Ref 4:746)
Continuous curve is for sample with carbon content of 2×10^{18} per cm^3.
Dashed curve is for sample with carbon content less than 10^{17} per cm^3.

The authors, however, did not recognize the sharp lines at a (1.26 microns) and c (2.54 microns) as zero-phonon lines. The energies of these lines correspond to the energies at which zero-phonon lines are seen in luminescence spectra at liquid nitrogen temperature (Ref. 22,33,41). The phonon-assisted sideband structure in the absorption spectrum is on the high energy side of the zero-phonon lines a and c. The broad band at b (1.69 microns) and the structure at d

(3.3 microns) had previously been seen in absorption spectra by Cheng et al. (Ref 9) and associated with the divacancy.

Luminescence Studies. Fig. 8 shows a luminescence spectrum of irradiated silicon reported by Panin et al. (Ref 30).

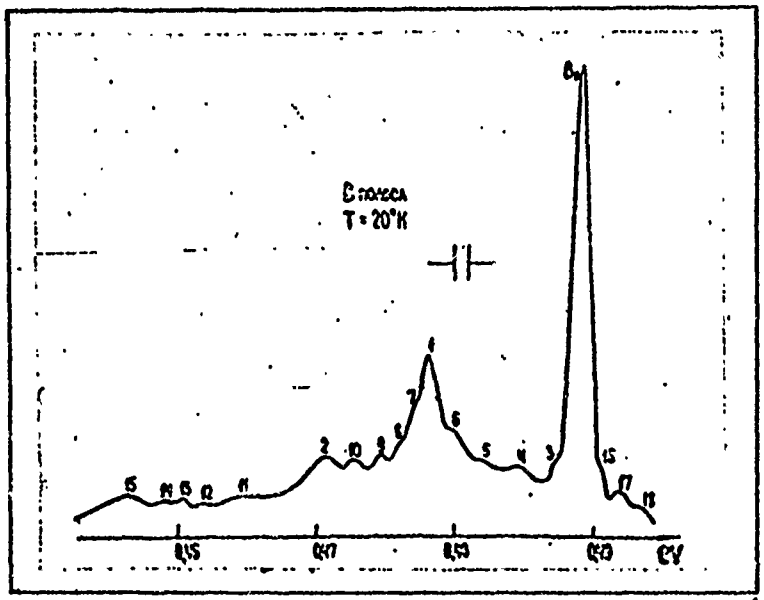

Fig. 8. Luminescence Spectra of Irradiated Silicon (Ref 30:6)

The spectrum indicates a sharp line at 0.490 eV (Bo) and the phonon-assisted sideband with major peaks at 0.478 eV (B_1), 0.471 eV (B_2), and 0.456 eV (B_{15}). This spectrum was observed for n- and p- type samples of varying oxygen content.

The luminescence spectrum shown in Fig. 9 was reported by Jones and Compton (Ref 22) for an n-type (phosphorus doped) pulled silicon sample irradiated with 10^{17} e/cm^2 at 2.5 MeV. Jones and Compton identified zero-phonon lines at 0.717 eV (A), 0.724 eV (B), 0.790 eV (C), 0.795 eV (D), 0.898 eV (E), 0.941 eV (F), and 0.970 eV (G). The broad structures to

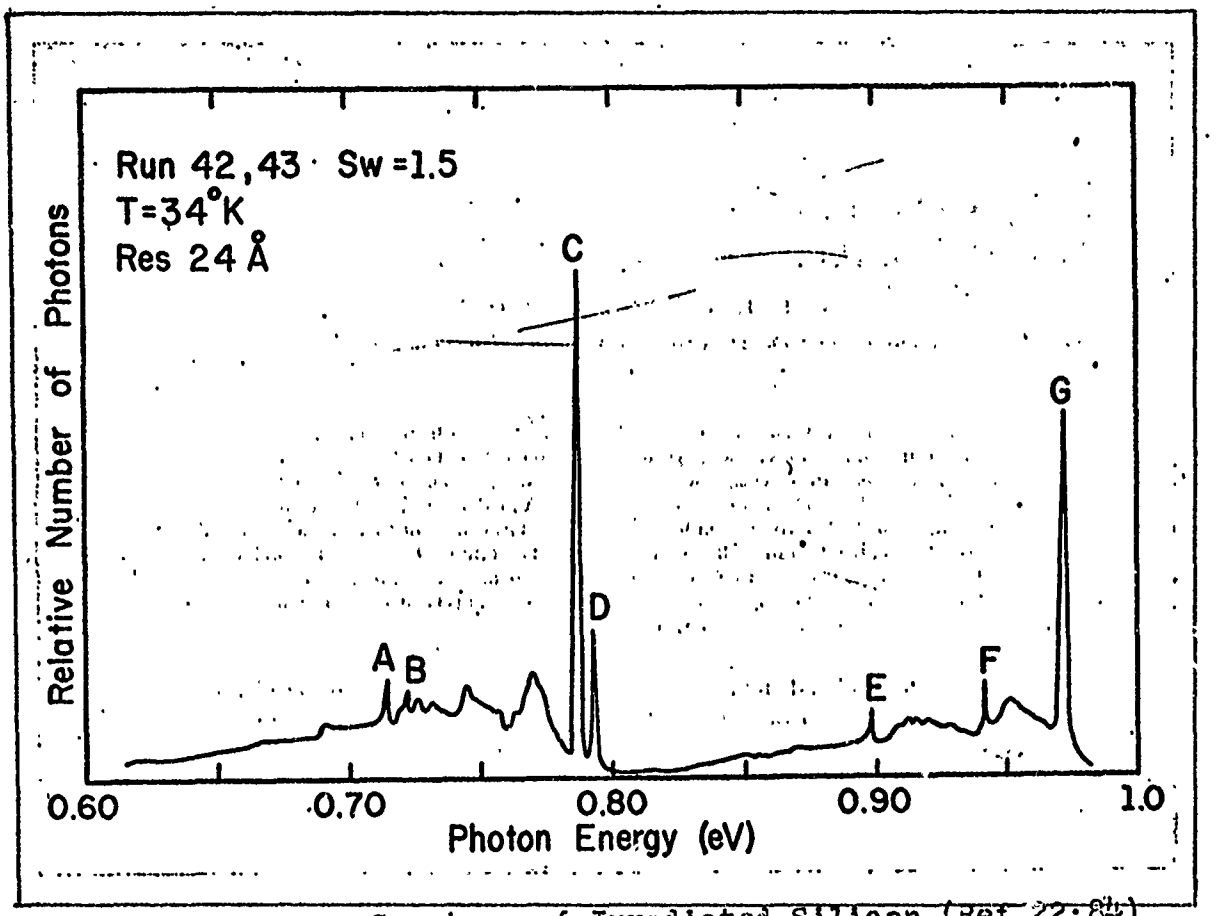

Fig. 9. Luminescence Spectrum of Irradiated Silicon (Ref 22:84). n-type pulled, 80 ohm-cm

the left of the strong lines C and G are the phonon assisted sidebands. The peak at 0.941 eV (F) was seen only in a few samples whereas the other structure between 0.80 eV and 1.0 eV always occurred in the same intensity ratios independent of any impurities (Ref 22:83). The structure below 0.80 eV was not seen in float-zone samples.

As seen in Fig. 9, the zero-phonon lines C and D form a doublet. Jones found (Ref 21:180) that the intensity of the line at 0.795 eV (D) was related to the line at 0.790 eV (C) by a Boltzmann factor. The high temperature intensity ratio was 1:1 (Ref 22:83). He concluded

that the lines are related to two levels of the initial state of the luminescence, i.e. the excited states.

The two luminescence spectra in Figs. 8 and 9 will be compared with the absorption spectra obtained in this study.

Table I, though not all inclusive, lists some previously reported zero-phonon lines which occur in the spectral range of this study. The table includes the temperature at which the spectrum was recorded. Some of the energy locations, which were not listed in the text of the reference, were measured from the appropriate spectrum.

Table I

Luminescence Zero-Phonon Lines

Note: Legend for table
n-n-type silicon
p-p-type silicon
C-Czochralski grown silicon
F-float zone grown silicon
e-electron bombardment
γ-Cobalt-60 gamma ray bombardment
LH-liquid helium

Line	Material class	Temperature (°K)	Irradiation source	Reference[a]
0.971	npCF	6.8	γ	33
0.971	np	20.4	e	30
0.970	npCF	11.8	e	20
0.970	npCF	34	e	22
0.969	nC	LH	e	b
0.967	npC	80	γ	40
0.797[c]	np	80	γ	6
0.795	npC	34	e	22
0.795	npC	11.8	e	20
0.794	nC	LH	e	b
0.794	nC	6.8	γ	33
0.791	npC	6.8	γ	33
0.790	npC	11.8	e	20
0.790	npC	34	e	22
0.790[c]	np	80	γ	6
0.790	nC	LH	e	b
0.490	np	20.4	e	30
0.489	nC	LH	e	b
0.488	np	80	γ	41

a: refer to reference in bibliography
b: unpublished data by Spry using sample from same boule used in this project
c: line was not seen until annealing at 300°C

V. Equipment and Procedures

General Description

The experiments reported in this thesis involve the measurement of absorption spectra of irradiated silicon. An overall description of the experiment is presented here, with more detailed procedures being given in the sections to follow.

The samples used were cut from one Czochralski and one float-zone grown single crystal boules of silicon. The optical surfaces were polished and then trimmed to a specified size depending on the measurement technique to be used.

The samples were irradiated with 1 MeV electrons from a Van de Graaff generator. By passing cooling water through the sample holder, the irradiations were performed at 27° C. To ensure that damage was nearly uniform throughout the samples, each sample was irradiated equally on both sides. The fluence to which each side was irradiated was calculated from the average beam current, area of the beam spot, and the total irradiation time.

To obtain optical absorption measurements, the samples were mounted on a cold finger in an evacuated dewar. The initial measurement was made using the differential technique at liquid nitrogen temperature. The rest of the measurements were made with a liquid helium dewar using the single beam technique. The dewar was placed in the sample compartment of a double beam, Cary, Model 14 RI

Recording Spectrophotometer. The output signal was presented on a strip chart recorder.

The recorder indicated the absorbance ($\log \frac{I_o}{I}$) as a function of wavelength. After subtracting off the baseline absorbance values, the set of data was punched on computer cards. The computer converted wavelength values to energy and generated an absorption spectrum through a plotting subroutine.

Sample Preparation

Slices of silicon were cut from the two boules with a diamond saw. Each face was polished with 0.5 micron diamond paste. The slices were trimmed to specified sizes and the cut samples marked with a letter designation and an arrow which was used to indicate the orientation of the sample. The theoretical per cent transmission is given by (Ref 27:14)

$$T = \frac{2n}{1 + n^2} \tag{11}$$

where n is the refractive index of silicon. The value of n used was 3.44 (Ref 18:439). A value of 53.8% transmission was obtained experimentally for the samples which compares well with the theoretically calculated value of 53.6%. Thus the faces of the samples were polished to give the theoretical per cent transmission.

The dimensions of samples A and B were 14.5 mm x 9.5 mm and 5.74 mm thick. These samples were purposely cut to this thickness to initially check if the absorption bands could

be detected by the Cary Spectrophotometer utilizing the differential technique.

It was determined that the use of the differential technique at 79°K was no more advantageous than the single beam method since there was no difference in the spectra recorded using either method. Use of the single beam method enabled measurements to be made at liquid helium temperatures. However, difficulties were encountered in mounting sample A in the liquid helium dewar. The sample was so thick that the brass thermal radiation shield would not fit over the cold finger. Instead, a piece of aluminum foil was wrapped around the cold finger to serve as a shield. Also, the temperature measuring diode could not be placed directly on the thick sample but had to be mounted on the opposite side of the cold finger.

With the encouraging results shown at liquid helium temperature utilizing the single beam method, the rest of the samples were cut to final dimensions of 9 mm x 9 mm and thicknesses less than 2 mm. A sample thickness of less than 2 mm was used so that the damage profile would be more uniform. The damage profile produced by 1 MeV electrons is a function of the electron range in silicon. Fig. 10 shows the damage profile produced in a piece of silicon where both sides are irradiated to equal fluences. The divacancy production per cm was used since this defect is the hardest to produce.

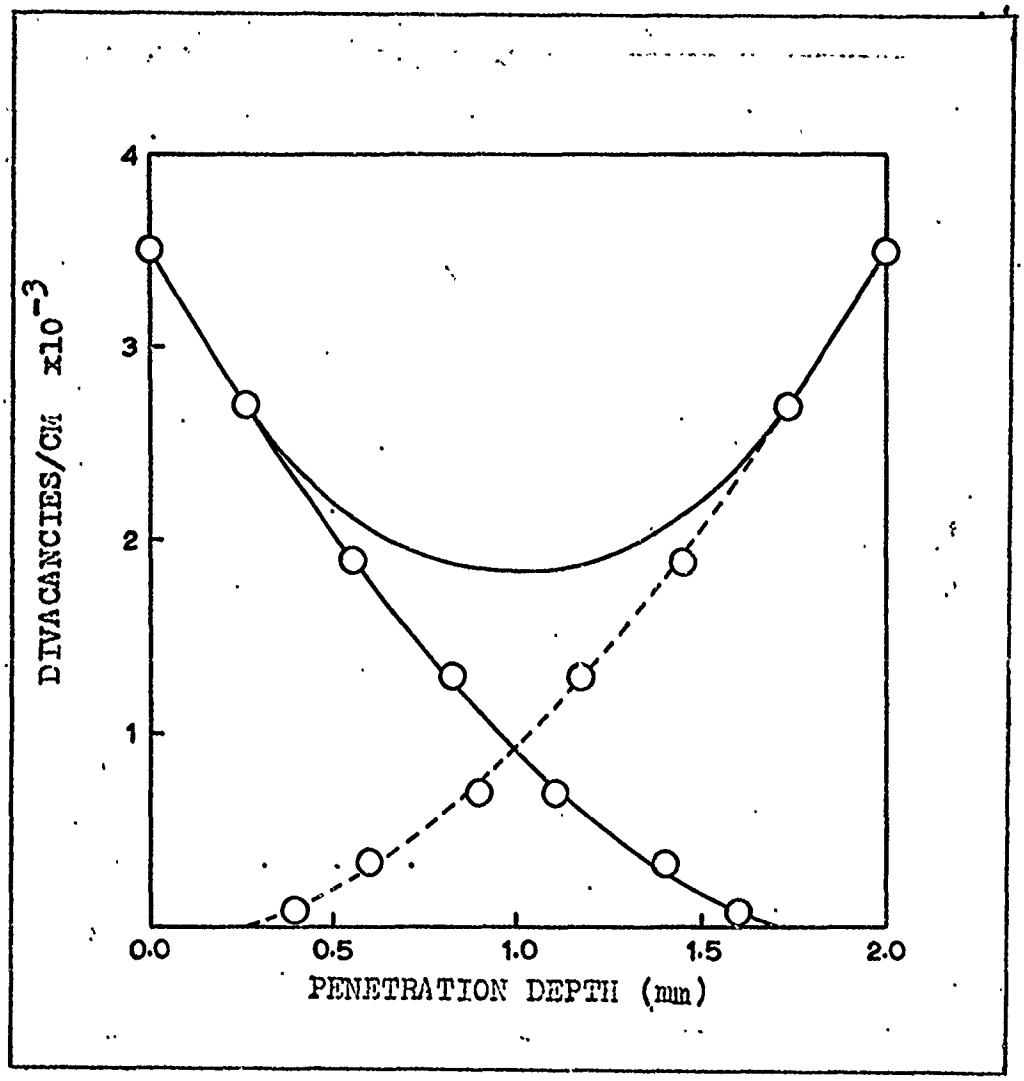

Fig. 10. Silicon Damage Profile for 1 MeV Electrons Data from Corbett (Ref 10:74). Each side irradiated to same fluence. Profile is composite of the two curves.

Table II lists pertinent information about the samples used in these experiments.

Table II

Silicon Sample Histories

Note: All samples were n-type (phosphorus doped) manufactured by Monsanto.

Designation	Growth method	Thickness (mm)	Resistivity (ohm-cm)	Electron fluence ($x10^{-18}$ e/cm^2)
A	pulled	5.74	40	4.6
B	pulled	5.74	40	none
E	pulled	1.73	40	0.5-7.6
H	pulled	1.68	40	5-7.6
O	pulled	1.69	40	4
X	float zone	1.89	120	2-4
Z	float zone	0.68	120	4-6

Sample Irradiation

The samples were irradiated with 1 MeV electrons from the Aerospace Research Laboratories Van de Graaff electrostatic generator. The samples were held in place by 2 copper clips which were attached by screws to the aluminum sample holder. The sample holder was cooled by water tubes connected to the closed-cooling system of the Van de Graaff diffusion pump. The sample temperature was monitored by a chromel-alumel thermocouple bead which was inserted into a small hole drilled half way into the sample holder. The hole was 1/8 inch from the sample holder face.

Fig. 11 shows a schematic of the irradiation sample holder.

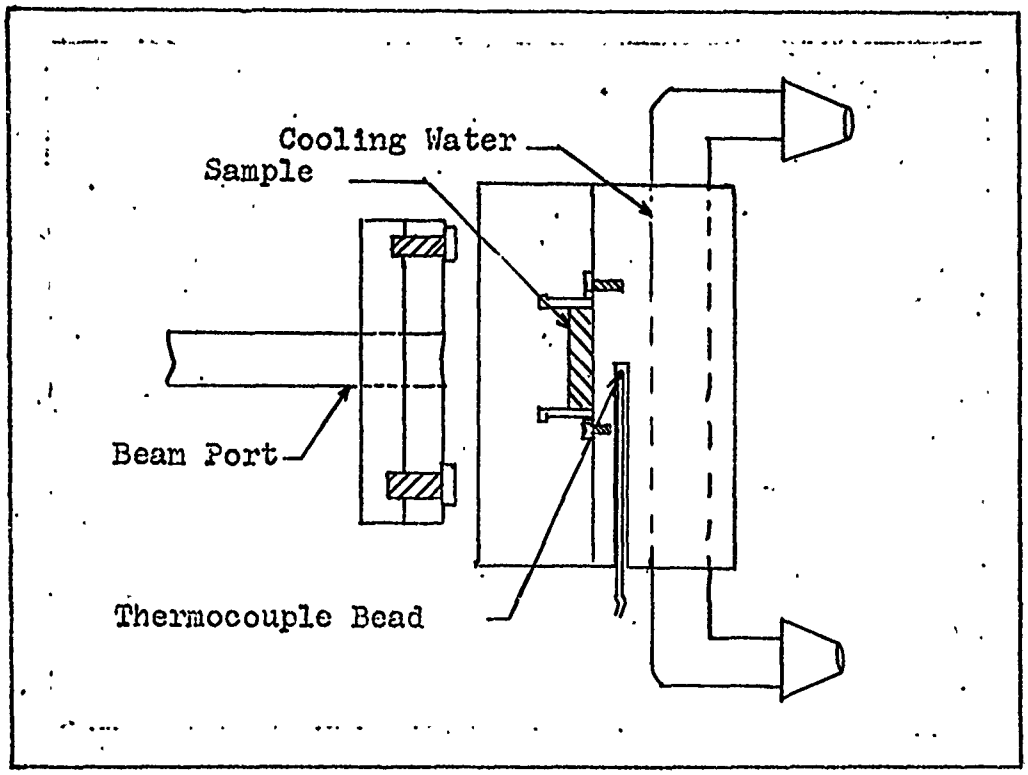

Fig. 11. Irradiation Sample Holder

The samples were irradiated using a beam current of 20 microamperes. The temperature of the sample remained about 4°C above room temperature. When the leading edge of the sample holder was placed about 3 mm from the beam port, the electron beam diameter was 5 mm corresponding to an area 0.196 cm^2. Because of this small beam area, the sample holder had to be positioned accurately to give a beam spot directly in the center of the sample. This was accomplished by first rough aligning the sample holder with no sample attached. A piece of ozalid paper, the size

of the sample, was placed in the center of the holder and "exposed" to the beam for 10 seconds. The paper was "developed" by holding it in ammonia vapor. The sample was then attached, and another piece of ozalid paper cut to the size of the sample was placed over the sample. A piece of thread was attached to one corner so that after the paper was exposed, it could be removed without disturbing the position of the sample holder. The time of exposure of the ozalid paper while on the sample was included in the total irradiation time. Each side of the sample was exposed to the full fluence value so that the damage would be more uniform.

The loss in beam energy was calculated to be 12 KeV. A 10 KeV loss resulted when the beam passed through a 1 mil thick aluminum foil (Ref 28:14) on the end of the beam port and a 2 KeV loss when it passed through 15 mm of air (Ref 28:21) before reaching the sample face. The beam current was monitored by attaching a lead to the Van de Graaff beam port and another to the sample holder. In this way the sample holder also functioned as a Faraday cup for collecting the incident electron beam.

The fluence to which each sample side was exposed was calculated as follows:

$$\phi = \frac{6.24 \times 10^{12} \, Bt}{A} \tag{12}$$

where ϕ is the electron fluence in electrons/cm^2, B is the average beam current during irradiation in microamperes,

t is total irradiation time in seconds, A is the area of beam spot in cm^2, and 6.24×10^{12} is a conversion factor (Ref 24 :31).

After irradiation, the samples were placed in containers and immersed in a mixture of dry ice and isopropyl alcohol to arrest room temperature annealing. The temperature of this mixture was about 195° K. The samples remained in this solution at all times except for optical absorption measurements and further irradiations.

Dewars

Liquid Helium Dewar. The liquid helium research dewar used in this experiment was a standard fixed temperature dewar with a hollow copper cold finger made by Sulfrian Cryogenics, Inc., Rahway, New Jersey. Sapphire windows were installed in the entrance and exit ports of the tail section. A copper platelet with a 6 mm square hole cut out of the center, was used as a mount for the sample. A piece of aluminum foil with a 4 mm diameter hole cut out was used to mask a small area of the sample. The mask was mounted between the cold finger and copper platelet with each surface coated with a thin layer of silver-loaded vacuum grease.

After the platelet and mask were attached to the cold finger, the silicon sample was removed from the dry ice-alcohol solution and mounted with silver-loaded vacuum grease. A phosphor-bronze clip was attached to the bottom of the cold finger to keep the sample from slipping down

when the dewar was in the upright position. Another clip, which had the gallium-arsenide diode expoxied on it, was positioned to rest on the sample, but not in the path of incident radiation, as shown in Fig. 12. The diode clip was attached to the cold finger with a screw which also held the copper platelet secure.

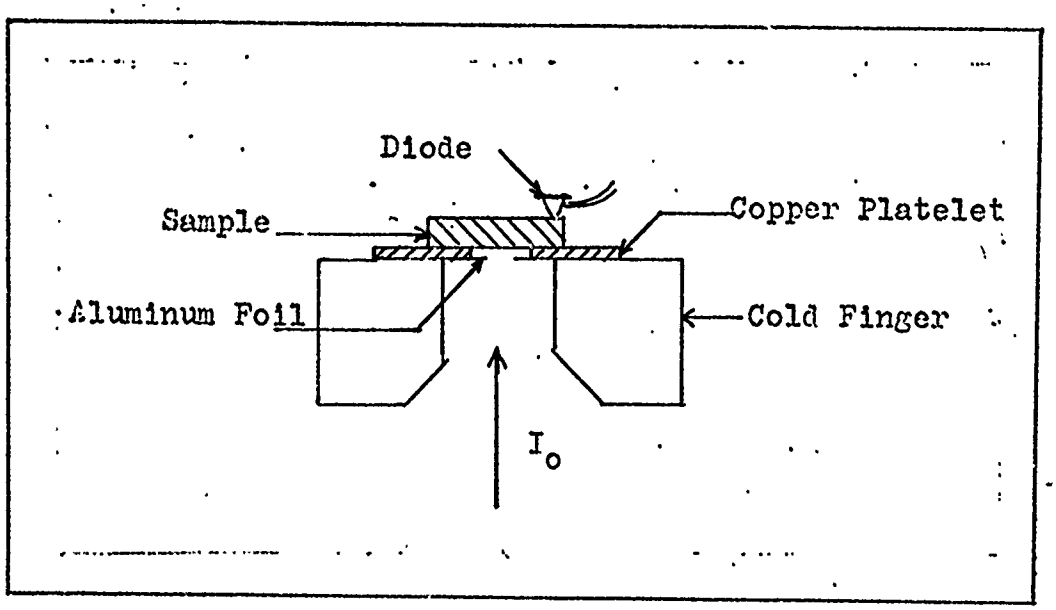

Fig. 12 Sample Mounting

Liquid Nitrogen Dewar. The liquid nitrogen dewar used in this experiment was manufactured by the Air Force Materials Laboratories Metal Shop. Sapphire windows were used in the entrance and exit ports of the tail section. The sample was mounted on a copper platelet with aluminum mask as in the helium dewar. However, the temperature was monitored by a copper-constantan thermocouple bead

soldered to the copper platelet.

Absorption Measurements

Liquid Helium. When an equilibrium temperature was reached, usually about 9-10°K, the dewar was placed in the sample compartment of the Cary Spectrophotometer. An aluminum cylinder 7½ inches high was made to support the dewar. This gave an accurate alignment of the dewar in the center of the incident beam. A plate with the same size mask was placed in the reference compartment.

A constant current of 10 microamperes was supplied to the temperature measuring diode and the change in resistance was monitored by a voltage reading from a Leeds and Northrup Volt Potentiometer. The reading was converted to a temperature value from the diode calibration data supplied by Lake Shore Cryotronics, Inc., Eden, New York.

Liquid Nitrogen. The temperature was allowed to reach equilibrium, usually 78-79° K and then the dewar was mounted on a flat aluminum plate which fit over the sample compartment of Cary Spectrophotometer. The room temperature plate with same size mask was placed in the reference compartment. Temperatures were monitored periodically by recording readings from a Leeds and Northrup Volt Potentiometer. These were converted to temperature values from a standard thermocouple conversion table.

Independent of which dewar was used, an initial scan

was run at 100Å /sec from 3.0 microns until an absorbance value of 2 was reached. Then a scan at 25Å /sec was run while recording the slit width readings at each of the sharp absorption bands. Scans at slower speeds consitent with the instrumental resolution were run at the regions of the prominent absorption bands. A determination of the scanning speed is given in the next section.

Spectrophotometer

Absorption spectra of irradiated silicon samples were obtained with a Cary, Model 14 RI Recording Spectrophotometer. The instrument was manufactured by Applied Physics Corporation, Monrovia, California, a Varian Subsidiary. A simplified optical system schematic is shown in Fig. 13. The IR No. 1 (Infrared, Number 1) mode of operation was employed in obtaining all spectra in this experiment.

In the IR No. 1 mode of operation, energy from a Halogen quartz lamp was dispersed by a double monochromater consisting of a 30° fused silica prism in series with a 600 line/mm echelette grating. The monochromatic radiation alternately passed through the reference and sample compartments. The optical energy of the reference beam striking the lead sulphide detector was maintained constant by an automatic slit servomechanism. The optical energy of the two beams striking the detector were converted to an electrical signal, amplified, and the ratio of the sample-to-reference signal was presented on a strip-chart recorder. The detailed operation of this

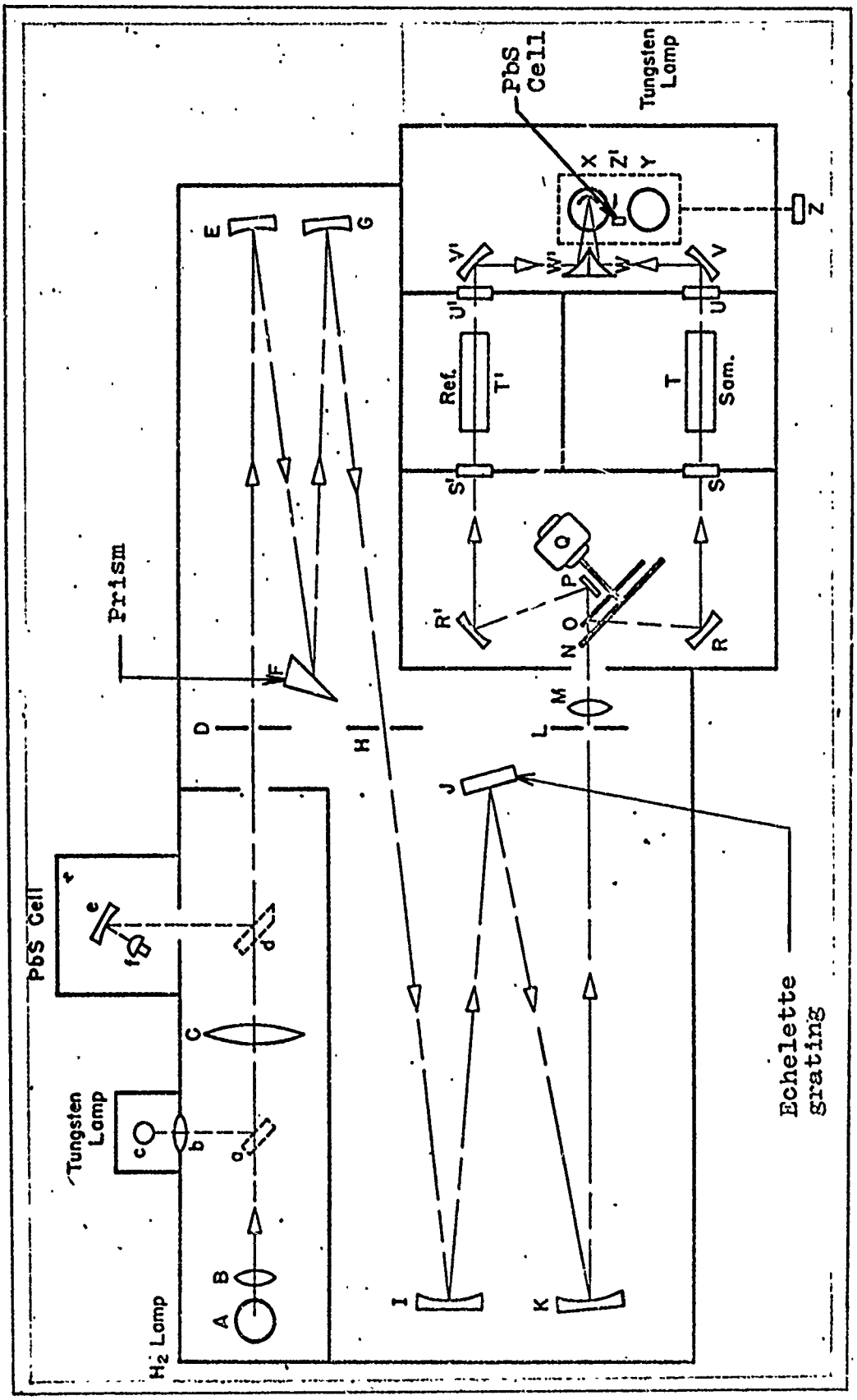

Fig. 13 Cary 14 Optical System
Light path for IR No. 1 shown

spectrophotometer can be found in the instruction book for the Cary, Model 14 RI (Ref 2).

Standard instrument settings were used to obtain the IR No. 1 mode of operation. The four adjustable control settings are described in the following paragraphs.

The Balance Control was initially set for an approximately zero absorbance reading when the liquid nitrogen dewar, without a sample, was placed on the sample compartment. A plate, with an aluminum mask with 4 mm diameter hole cut in the center, was placed in the reference compartment. The strip chart recording of this absorbance versus wavelength was the baseline spectrum. However, when measurements were taken at liquid helium temperatures, the absorption bands of the sample were off scale. The Balance Control was set to bring these bands on scale. This in effect set up a new baseline which had to be recorded at liquid helium temperature. This was done in the same manner as was previously described. Since it was possible to also make measurements at liquid nitrogen temperature with the liquid helium dewar the small liquid nitrogen dewar was no longer used.

The voltage setting for the energy source transformer was 70 volts. This setting was used for it was found experimentally to give the best instrumental resolution.

The Slit Control Knob was set at a zero setting on the instrument panel. This knob controlled the signal amplification for the automatic slit control servomechanism.

As mentioned before, the optical energy of the reference beam striking the detector was maintained constant by automatically opening or closing the slits.

The Slit Height Knob actuated a mask which allowed continuous slit height adjustment from a maximum of 20 mm to a minimum of 7 mm. The slit servomechanism automatically adjusted the slit width to maintain constant energy striking the detector. The aperture area remained constant so that the 20 mm slit height resulted in a smaller slit width. A smaller slit width in turn resulted in a better instrumental resolution. This control was initially set at a setting of 7 mm for the first spectra recorded for sample A. After that it was set at 20 mm for the remainder of the experiment to optimize the instrumental resolution.

The instrumental resolution for the two slit heights are plotted in Fig. 14. The values were determined by taking the slit width reading in mm at a specified wavelength and multiplying by the reciprocal dispersion as read from the Resolution Data curve in the Cary instruction book (Ref 2).

The spectrophotometer was calibrated with the 10,140Å and 15,295Å mercury lines from a Pen-Ray qwartz lamp. The wavelength scale was found to be high by a vlue of 4Å at 1.01 microns and 3Å at 1.53 microns. The wavelength readings recorded from the strip chart recording were corrected by subtracting 3Å. Since the halfwidths of the mercury lines are much smaller than the typical resolution values

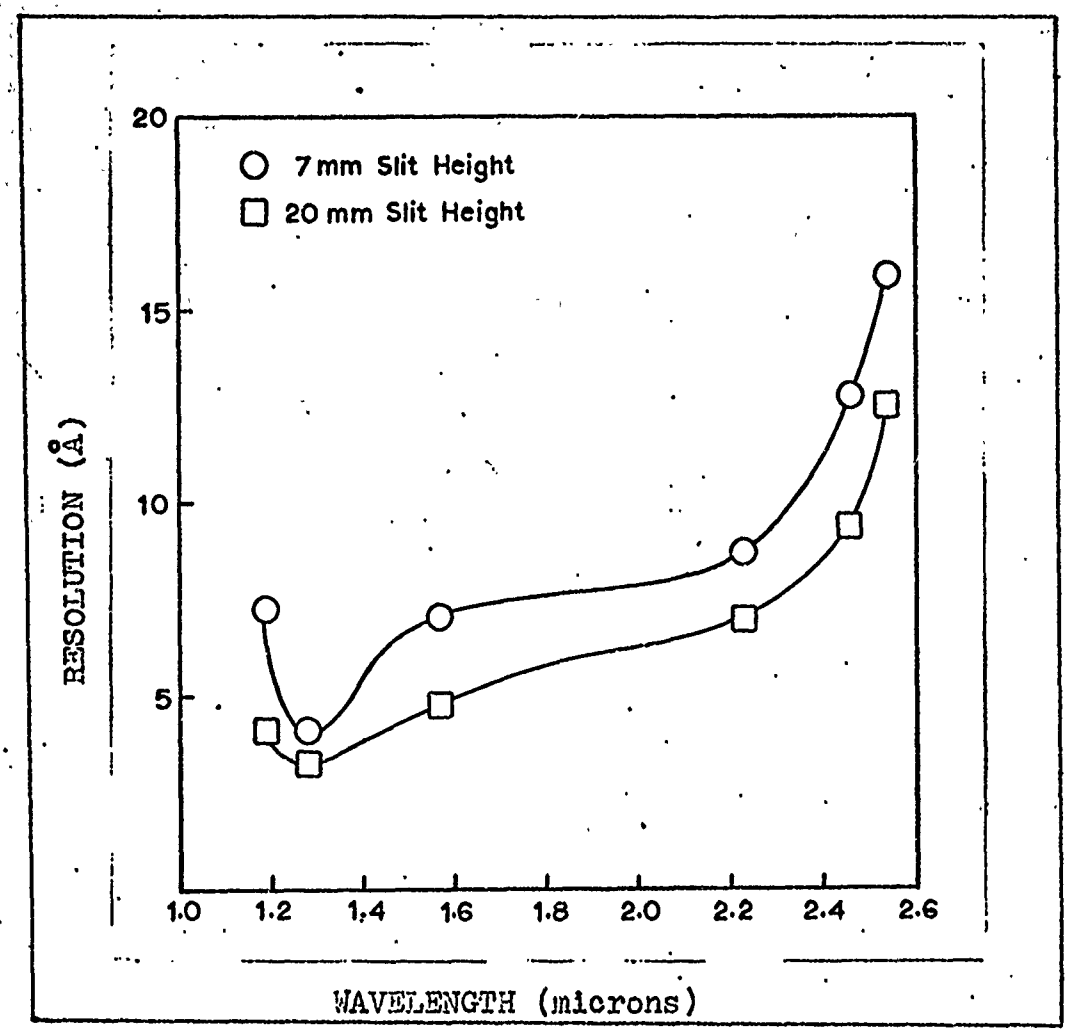

Fig. 14 Instrumental Resolution for Different Slit Heights

measured in this study, a measurement of the halfwidths of these lines will give the instrumental resolution. The measured halfwidths for the two mercury lines are shown in Figs. 15 and 16 along with the calculated instrumental resolution values. The resolution in Å is plotted against slitwidth in mm and extrapolated to the longest value of the slitwidth used. The ratio of the measured resolution (mercury line) to the calculated resolution was used as a correction factor for the resolutions given in Fig. 14.

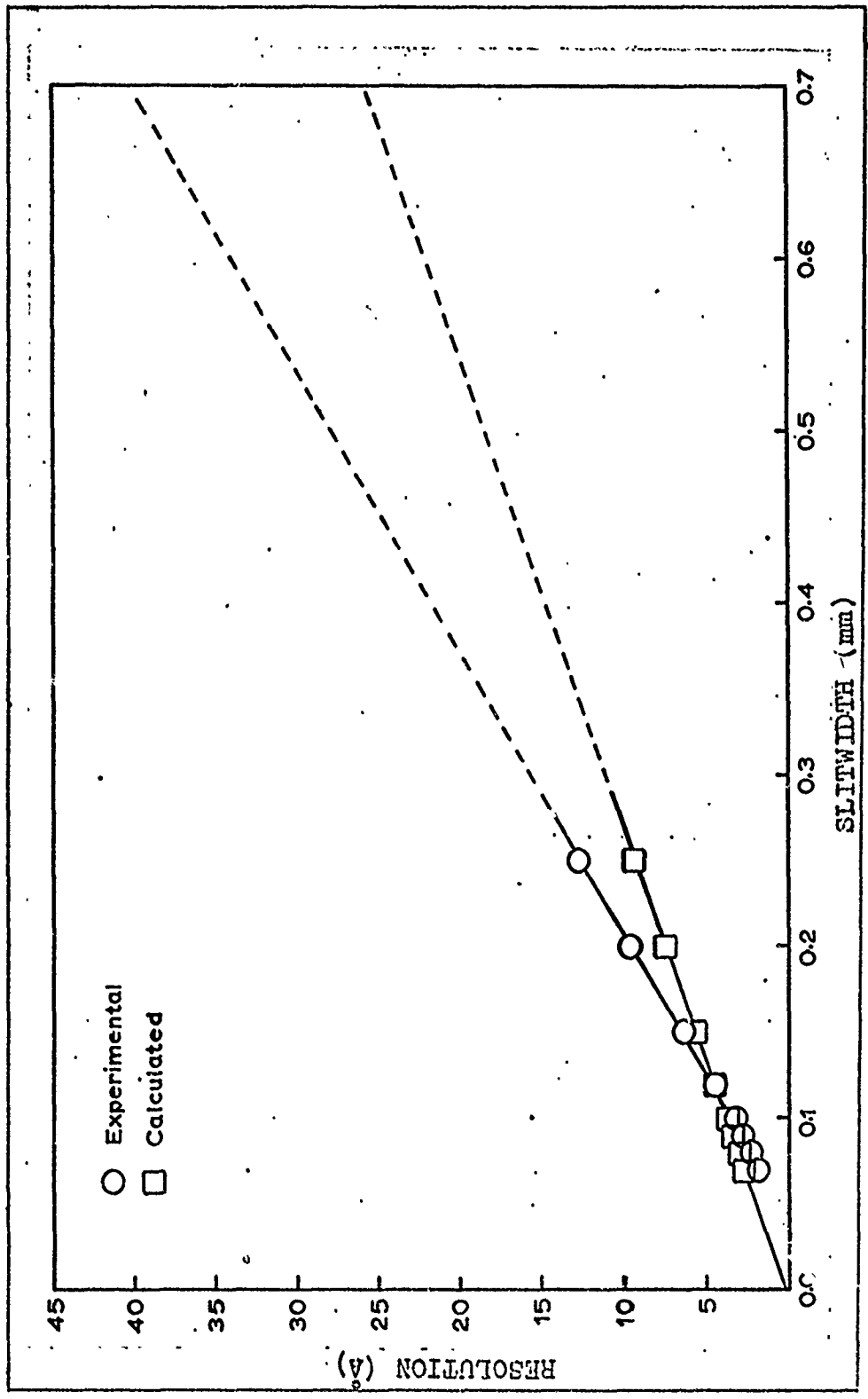

Fig. 15. Experimental and Calculated Resolution for 10140Å Line

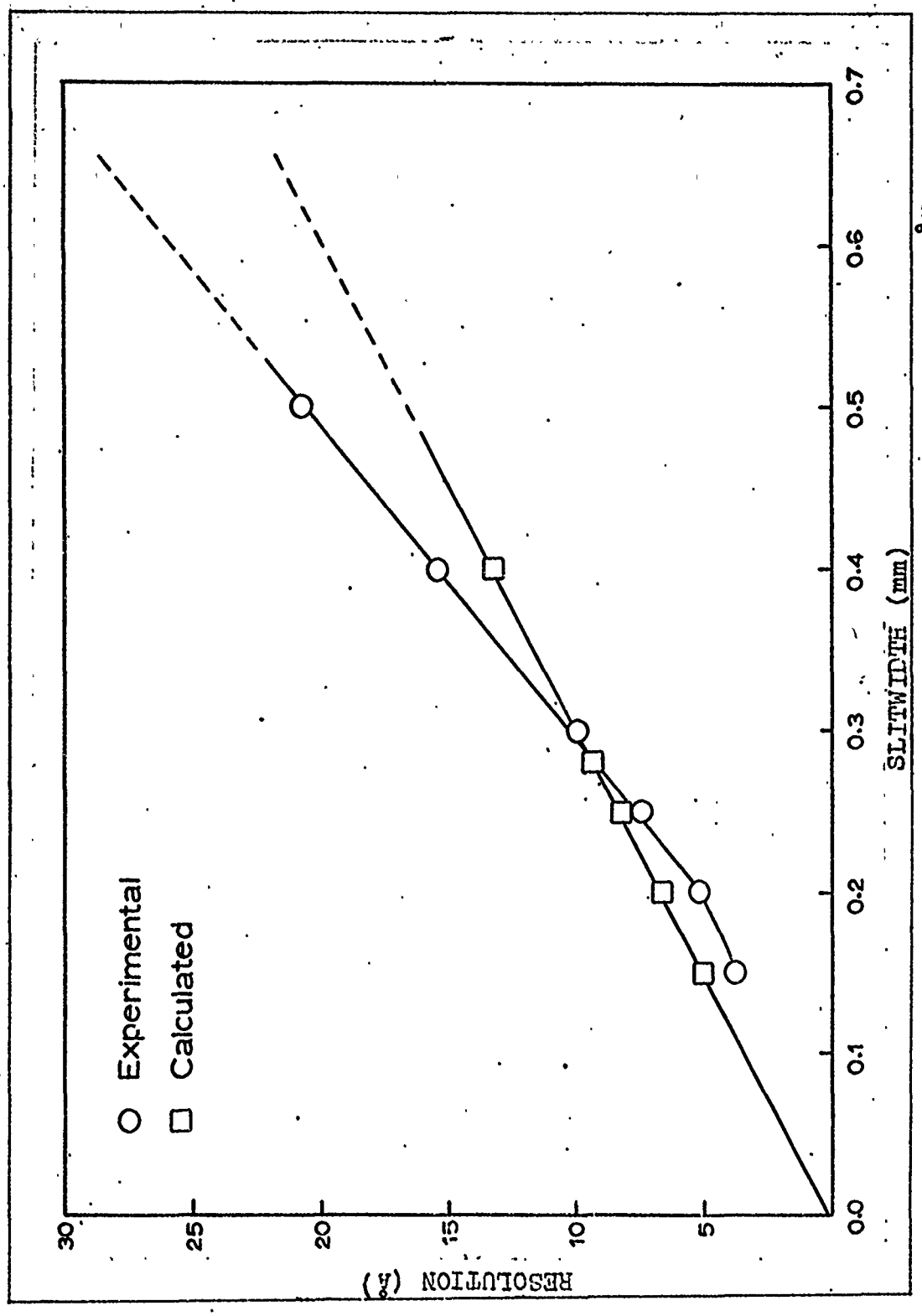

Fig. 16. Experimental and Calculated Resolution for 15295Å Line

According to Seshadri and Jones (Ref31:1039) a distortion is introduced into the shape of an infrared absorption band by an RC filter network. The qualitative results from their analysis is that an increase in the scanning speed reduces the relative peak height value, broadens the absorption band, and displaces the band maximum in the direction of scan.

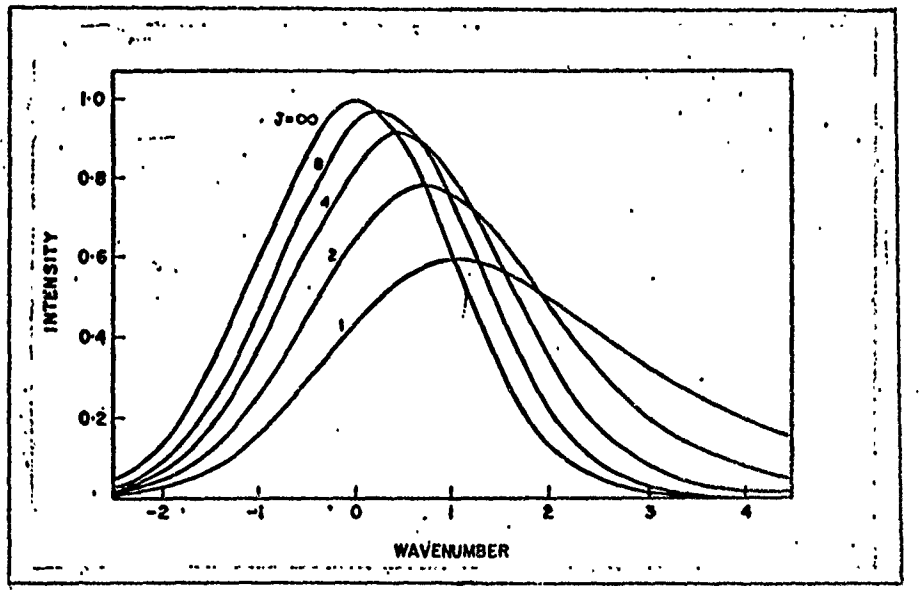

Fig. 17. Distortion in Gaussian Profile (Ref 31)

This distortion, as shown in Fig. 17, is characterized by a value J. The value of J is given by

$$J = \frac{\delta t}{\tau} \tag{13}$$

where δt is the input pulse width and τ is the filter time constant. The input pulse width may be written as

$$\delta t = \frac{\Delta \lambda}{d\lambda/dt} \tag{14}$$

where $\Delta\lambda$ is the instrumental resolution and $d\lambda/dt$ is the scanning speed. For the Cary 14, the RC filter time constant was given by

$$\tau = \frac{T}{5} \tag{15}$$

where T is the pen period (Ref 2). The scanning speed for the Cary 14 was determined by dividing the instrumental resolution by the pen period, which was one second. Using equations (14) and (15), the value for this instrument was found to be J=5.

Data Processing

The output of the strip chart recorder was the absorbance versus the wavelength in microns. To obtain a spectrum to compare with luminescence spectrum this output data was fed into a computer which plotted the spectrum of absorbance versus photon energy.

To obtain computer input data, the baseline absorbance values at specified wavelengths were subtracted from the irradiated sample absorbance values at the same wavelength. More points were taken around the peak absorption bands to define the true shape of the band. This information, the net absorbance and corresponding wavelength, were punched on computer cards. The computer converted wavelength to energy and, through a plotting subroutine, generated on absorbance spectrum.

Data for the dose rate studies were taken from the

strip chart output recorded for sample E. The intensity or height of the prominent absorption bands were measured after each integral increase in fluence. The height of the bands was used instead of the area for the halfwidth of the bands remained relatively constant. The height was plotted versus the electron fluence for each prominent band.

VI. Experimental Results

The experimental results will be presented in three sections; each section corresponding to one of the three expressed purposes of this project. The first section contains absorption spectra from an n-type, pulled silicon sample. The spectra indicate some bands previously seen in absorption studies and some structure that has not been seen before in absorption spectra. The next section will contain a comparison of the spectra obtained in this study with spectra obtained by recombination luminescence. Both the structure and energy of the bands will be compared. The final section will include the dose rate study conducted on one sample to determine which bands could be related and identified with a known defect.

Absorption Spectra

As mentioned before, the first purpose of this study was to obtain absorption spectra of electron irradiated silicon which showed the same narrow lines reported by Bean, et al. (Ref 4). Also, a search was to be made for the zero-phonon lines which occur in luminescence spectra of irradiated silicon (Ref20,22,30,33,41). The spectra obtained in this study did exhibit the narrow bands reported by Bean, et al. with the addition of narrow bands not seen in their spectra. Both the liquid nitrogen and liquid helium absorption spectra contained narrow bands and phonon-assisted sideband structure seen in luminescence spectra.

The spectra contained in this section were obtained from sample A, a Czochralski grown crystal. The pre-irradiation absorption spectrum is shown in Fig. 18. The sample temperature was 78.1°K. This spectrum illustrates the absorption edge of silicon at liquid nitrogen temperature.

Fig. 19 shows the irradiated absorption spectrum of sample A over the energy range 0.40 eV to 1.20 eV. The sample temperature was 79°K. In Figs. 20 thru 22 the energy scale has been expanded for this same spectrum. The expanded scale spectra give more detail and indicate the existence of three bands not seen in Fig. 19.

The natural band width was determined from the observed band width and the instrument resolution. This is possible if the measured band shape fits a known mathematical profile. According to Seshadri and Jones (Ref 31:1047), absorption band shapes commonly fit the Gauss, Cauchy, or Voigt forms. The experimentally observed band arises from the convolution of the true band profile and an instrument function. Assuming that the observed band shape and instrument function are both Gaussian, then the natural band width will be Gaussian. The natural band width is given by

$$NBW = \left[(OBW)^2 - (SBW)^2\right]^{\frac{1}{2}} \qquad (16)$$

where NBW is the natural band width, OBW is the observed band width, and SBW is the spectral band width or instrumental resolution. The natural band width may be converted

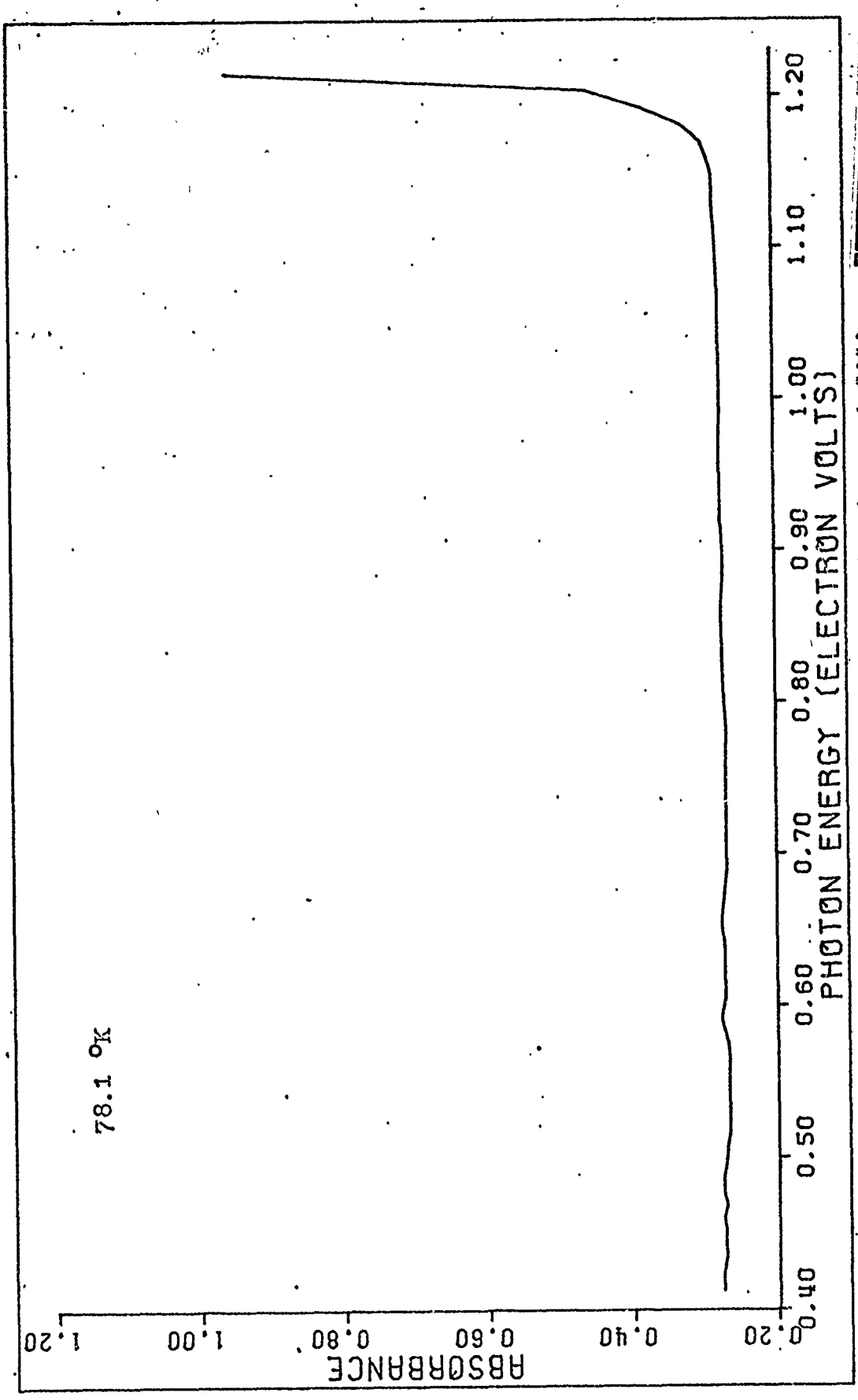

Fig. 13. Pre-Irradiation Absorption Spectrum of Silicon Sample A, n-type pulled, 40 ohm-cm.

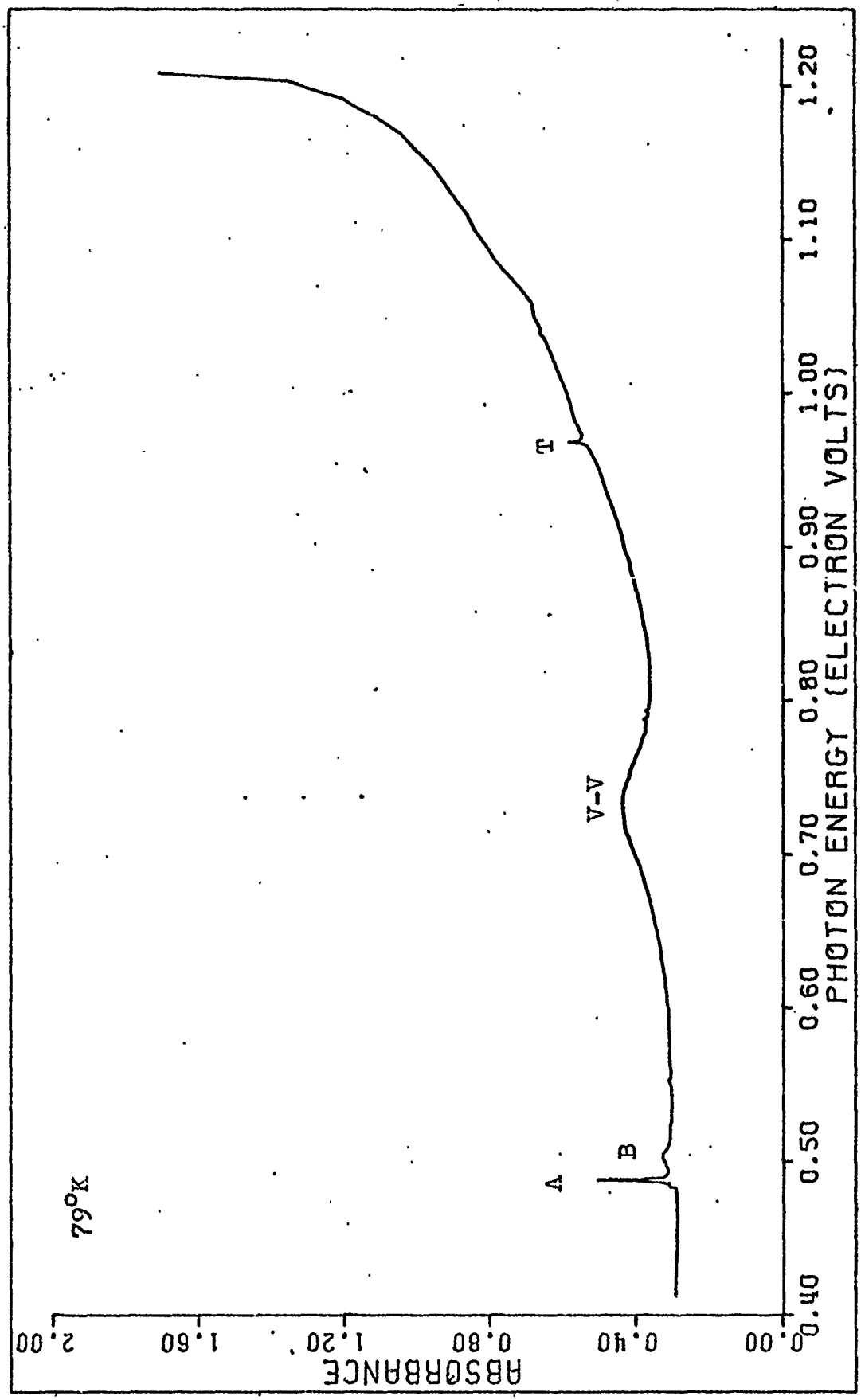

Fig. 19. Absorption Spectrum of Electron Irradiated Silicon Sample A, n-type pulled, 40 ohm-cm. Energy range 0.40 eV to 1.20 eV.

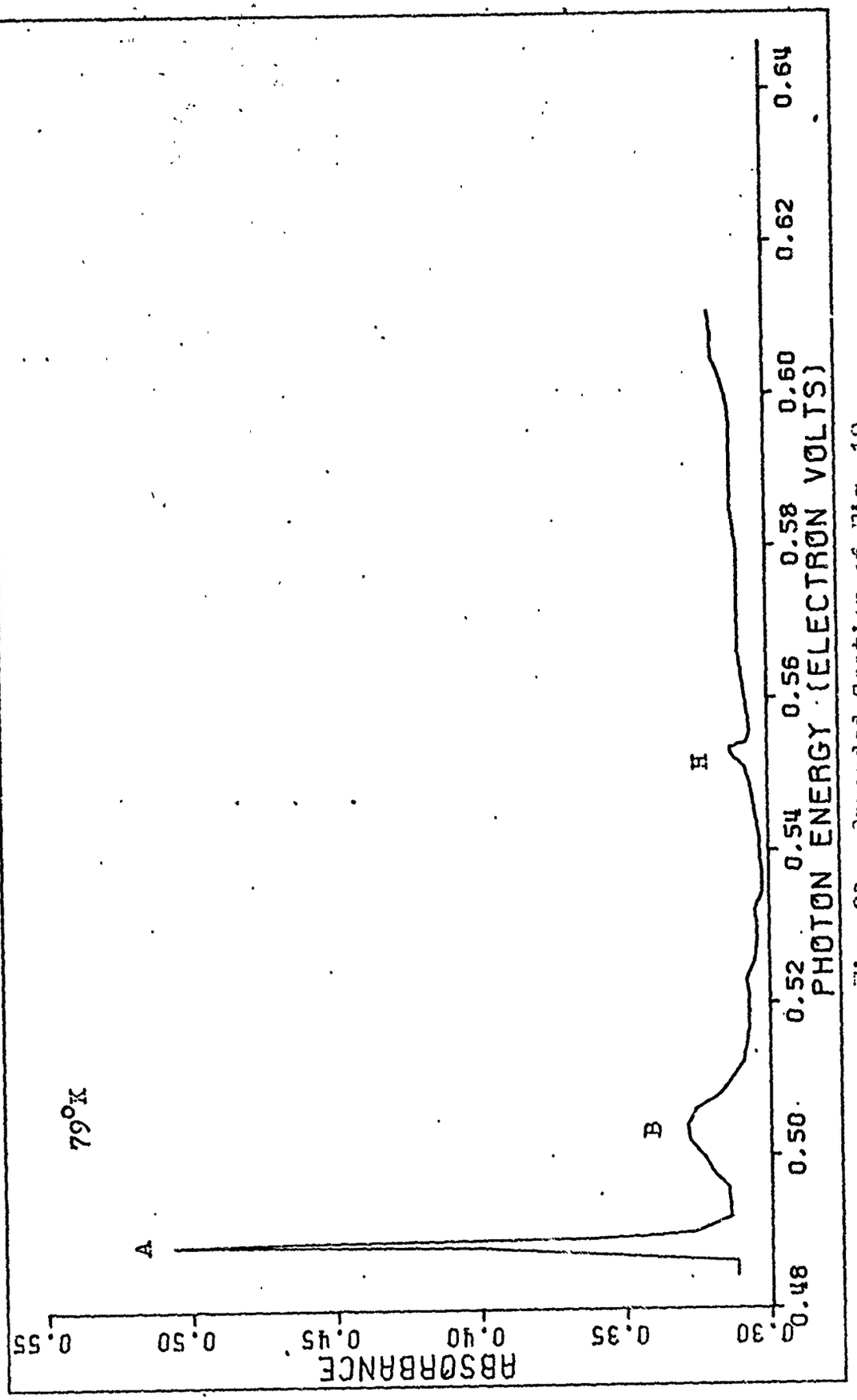

Fig. 20. Expanded Section of Fig. 19
Energy range 0.48 eV to 0.61 eV

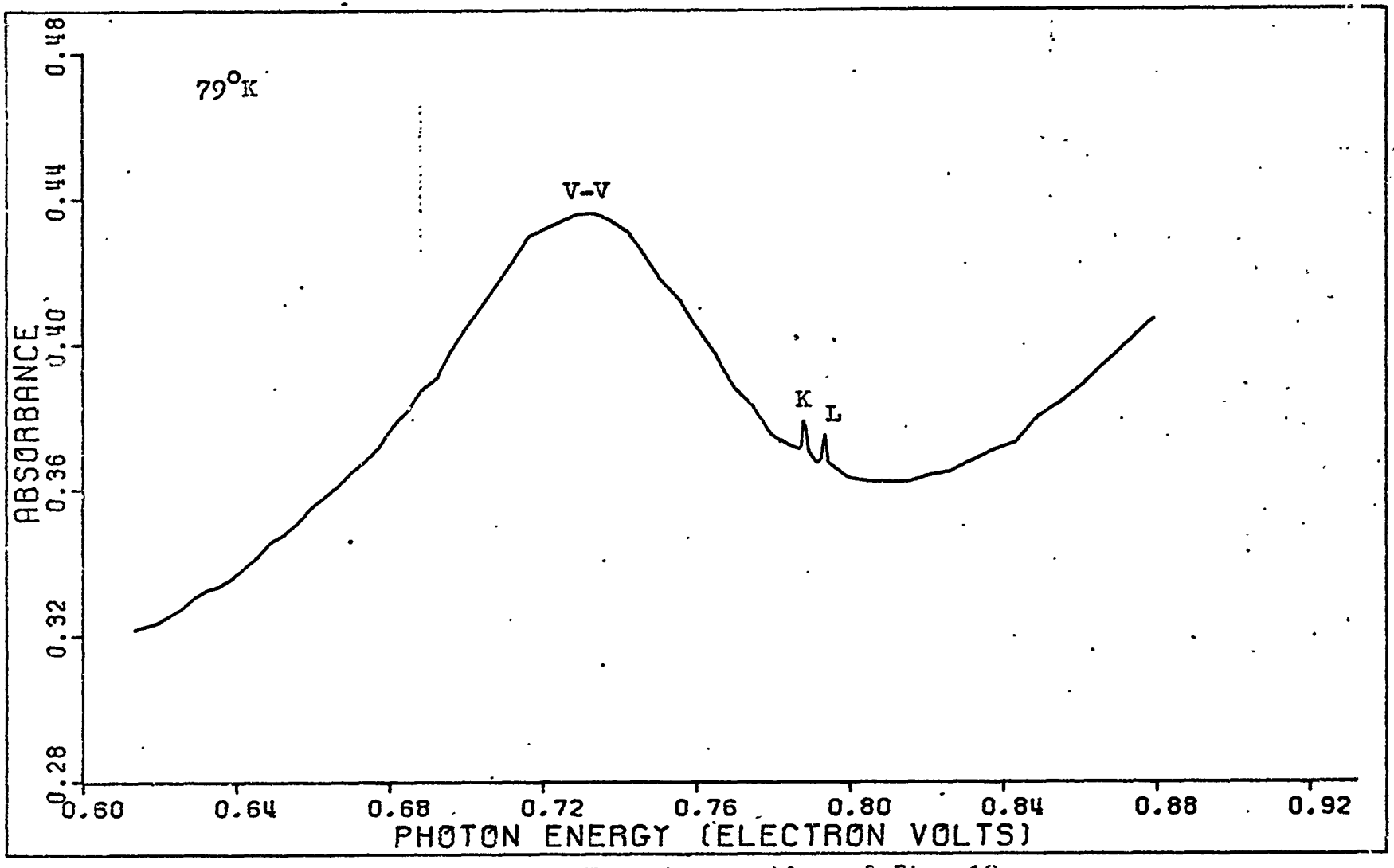

Fig. 21. Expanded Section of Fig. 19
Energy range 0.60 eV to 0.88 eV

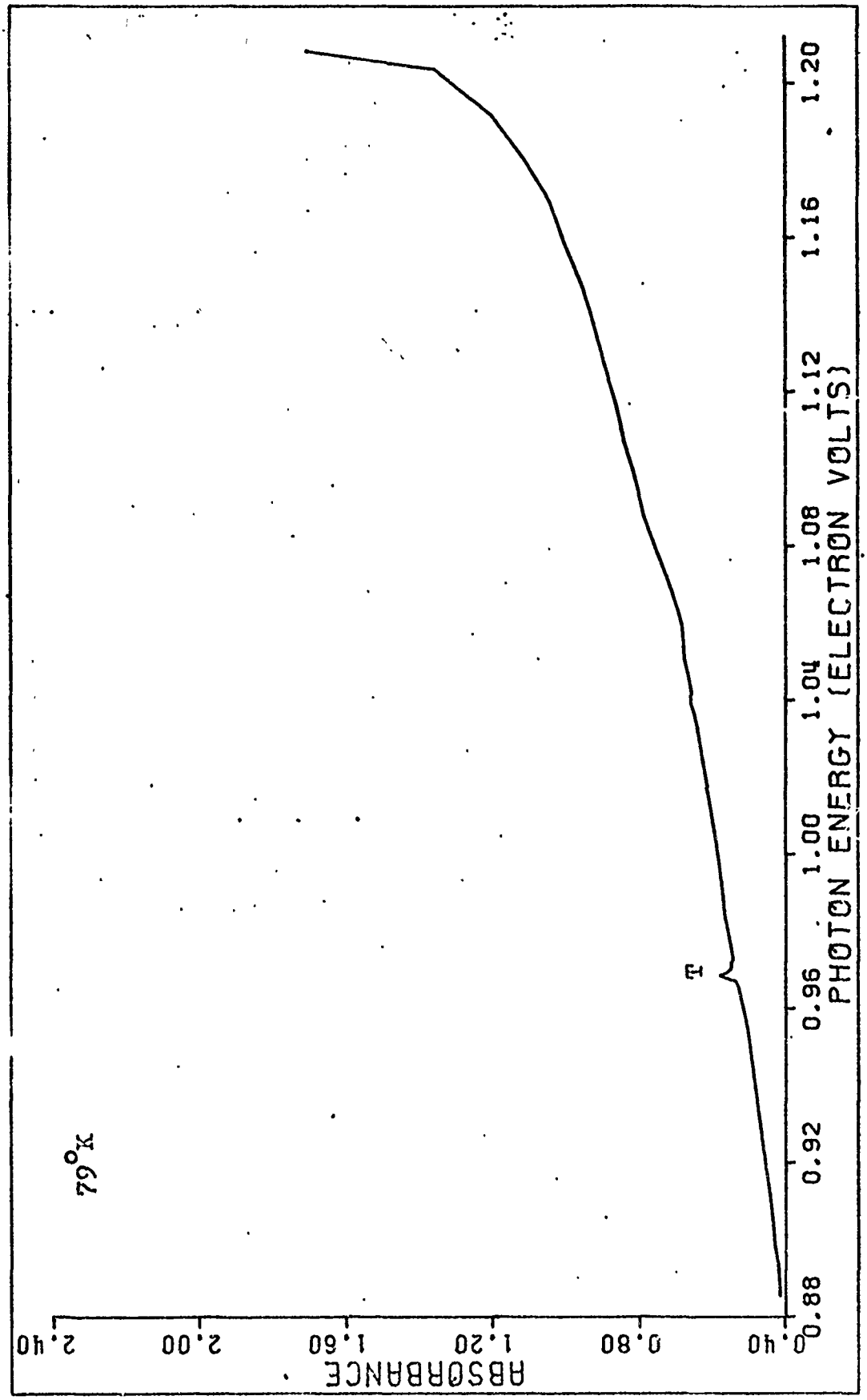

Fig. 22 Expanded Section of Fig. 19
Energy range 0.88 eV to 1.20 eV

to energy units according to the relation

$$\Delta\Sigma = \frac{1.24\Delta\lambda}{\lambda^2} \qquad (17)$$

where Σ is in eV, λ is wavelength of the band peak in microns, and $\Delta\lambda$ is the natural band width in microns.

The letter designation assigned to these bands along with their wavelength location, corresponding energy, and band widths are listed in Table III.

Table III

Absorption Bands at Liquid Nitrogen Temperature

Note: OBW-observed band width
SBW-spectral band width (instrumental resolution)
NBW-natural band width

Band	Wavelength (micron)	Energy (eV)	OBW (Å)	SBW (Å)	NBW (Å)	NBW (meV)
A	2.537	0.4887	54	16.1	51.5	0.99
B	2.464	0.5032	378	11.3	378	7.72
H	2.241	0.5533	87	6.9	86.7	2.14
V-V	1.695	0.7315	1920	6.6	1920	82.9
K	1.572	0.7888	24	3.8	23.7	1.19
L	1.562	0.7938	29	3.8	28.8	1.46
T	1.280	0.9687	23	2.8	22.8	1.73

The spectra in Figs. 19 thru 22 indicate the existence of three absorption bands not seen in the spectra reported by Dean, et al. in Fig. 7. These bands are located at 0.5533 eV (H), 0.7888 eV (K), and 0.7938 eV (L). However,

two bands shown in Fig. 7 were not seen in Figs. 19 thru 22. Band d at 3.3 microns was not observed in these spectra for it was not within the spectral range examined in this study. The Cary 14 had an upper spectral limit of 3.0 microns and comparisons were to be made with luminescence spectra which did not extend to that wavelength. The band at 1.262 microns in Fig. 7 was also not observed at 79°K. Although a band at that location did appear as will be seen in the spectra recorded at 11.5°K, it could not be discerned from the background at 79°K.

A comparison of the results reported by Bean, et al. with those found in this study is given in Table IV.

Table IV

Liquid Nitrogen Absorption Spectrum Comparison

Note: The energy values listed for Bean, et al. were converted from wavelength locations.

Band[a]	Wavelength (microns)	Energy (eV)	Band[b]	Energy (eV)
a	1.284	0.9657	T	0.9687
b	1.689	0.7341	V-V	0.7315
	2.467	0.5026	B	0.5032
c	2.541	0.4879	A	0.4887

a: spectrum in Fig. 7
b: spectra in Figs. 19 thru 22

The absorption spectrum for sample A was recorded at liquid helium temperature in order to search for other phonon-assisted side band structure present in luminescence spectra at that temperature. This spectrum is shown in Fig. 23. The expanded scale spectra are shown in Figs. 24 thru 26. These spectra show the existence of eleven bands which were not seen at liquid nitrogen temperature. All of the bands found at liquid helium temperature are listed in Table V on page 64. Included are the wavelength location, energy, and band widths.

All of the narrow bands observed at 79°K were shifted to shorter wavelength locations at 11.5°K and therefore higher energy values. This shift toward shorter wavelength locations (higher energy) was due to the variation in the silicon energy gap as a function of temperature. As the temperature decreases, the silicon band gap increases. The energy separation between bands K and L was 5 meV. As seen in Fig. 25, the structure on the high energy side of these bands seem to occur in pairs. The energy separation between the pairs M-N and O-Q is 5 meV also.

The results presented thus far have all been from the spectra of sample A. As mentioned in chapter V, this sample was cut thicker than that used by Bean, et al. or any of the investigators who used recombination luminescence to study radiation defects. Since a thinner sample can be more uniformly irradiated, a float zone crystal, sample Z, was cut to a thickness of 0.68 mm. The float zone sample

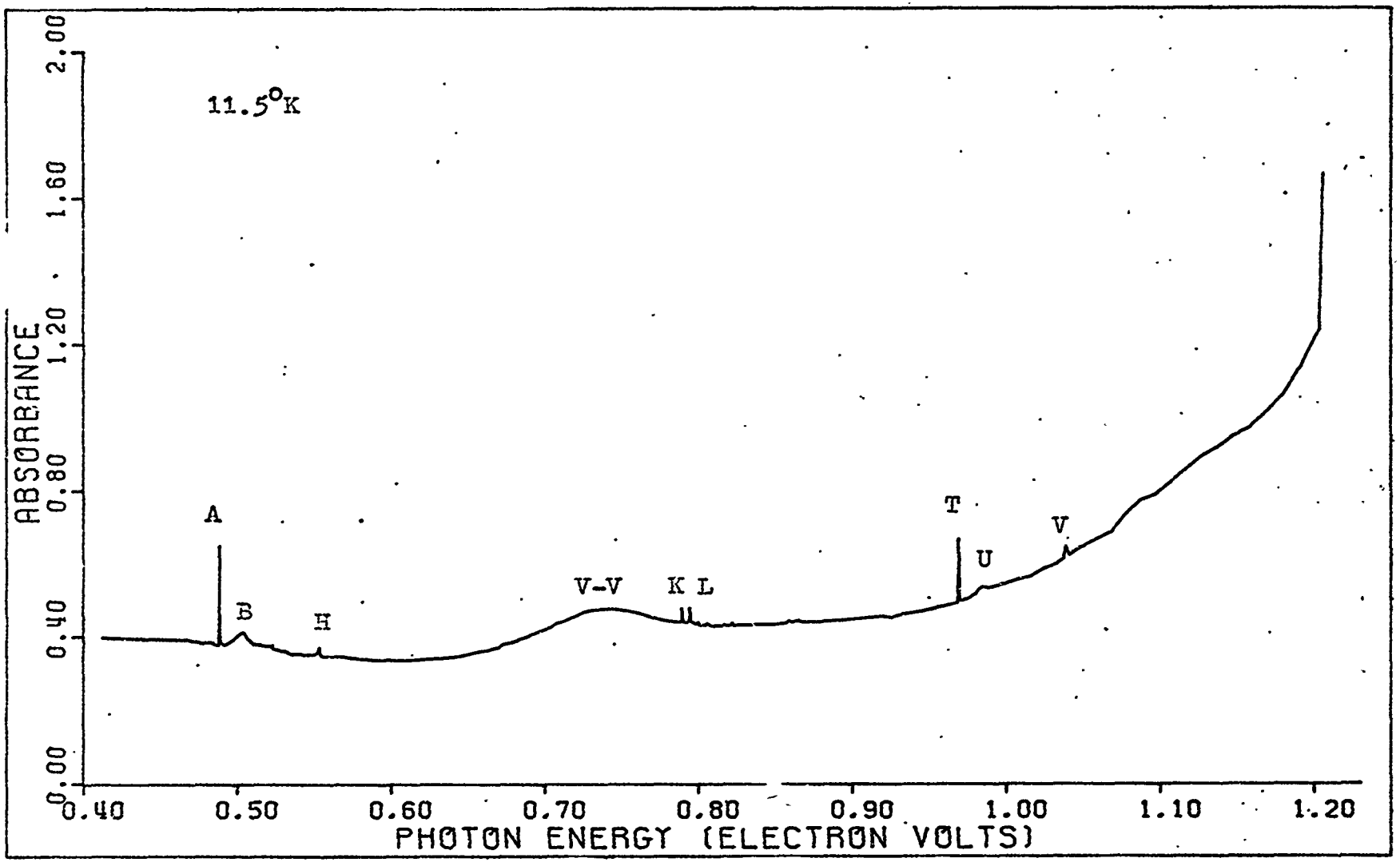

Fig. 23. Absorption Spectrum of Electron Irradiated Silicon Sample A, n-type pulled, 40 ohm-cm Energy range 0.40 eV to 1.20 eV

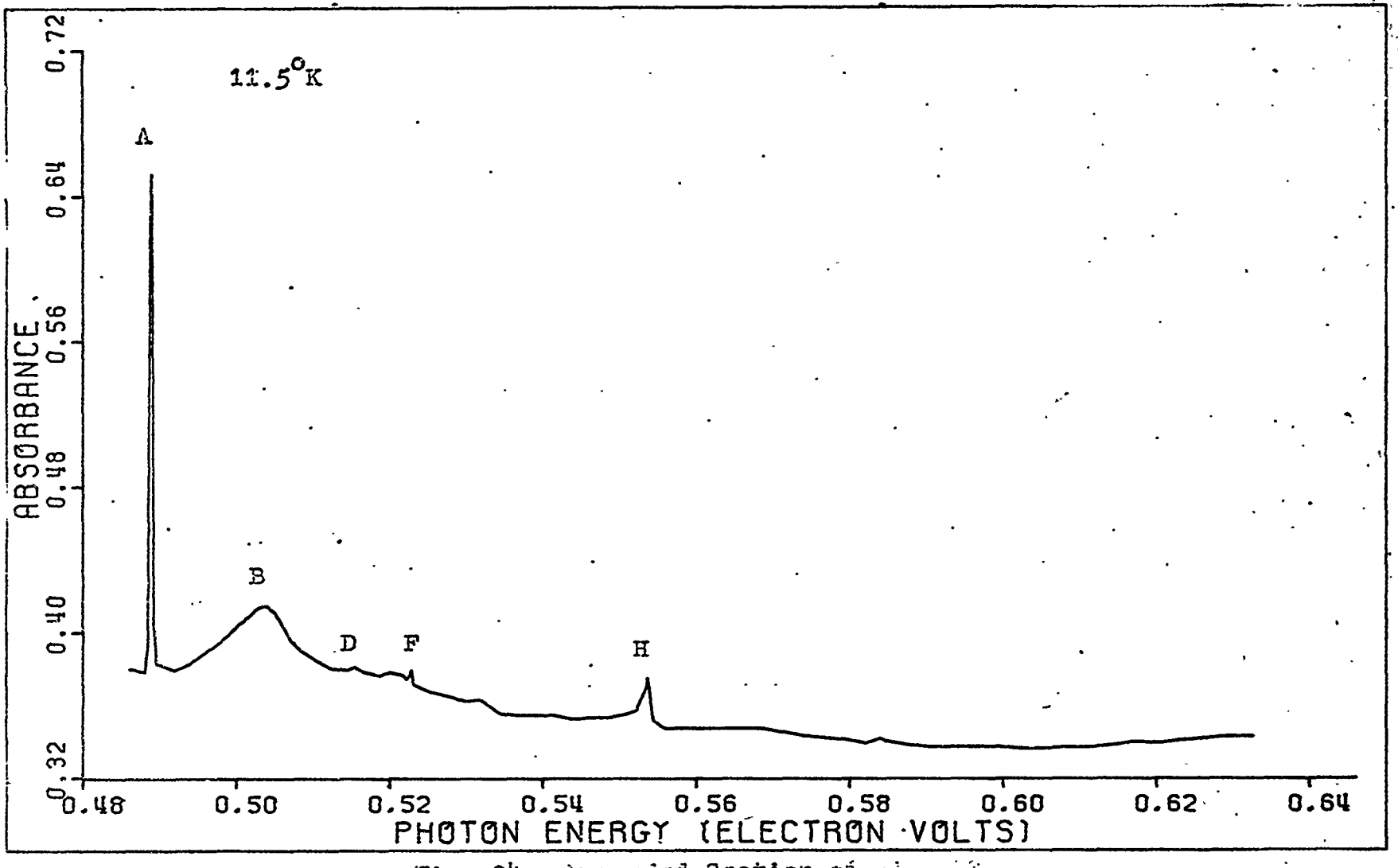

Fig. 24. Expanded Section of Fig. 23 Energy range 0.48 eV to 0.63 eV

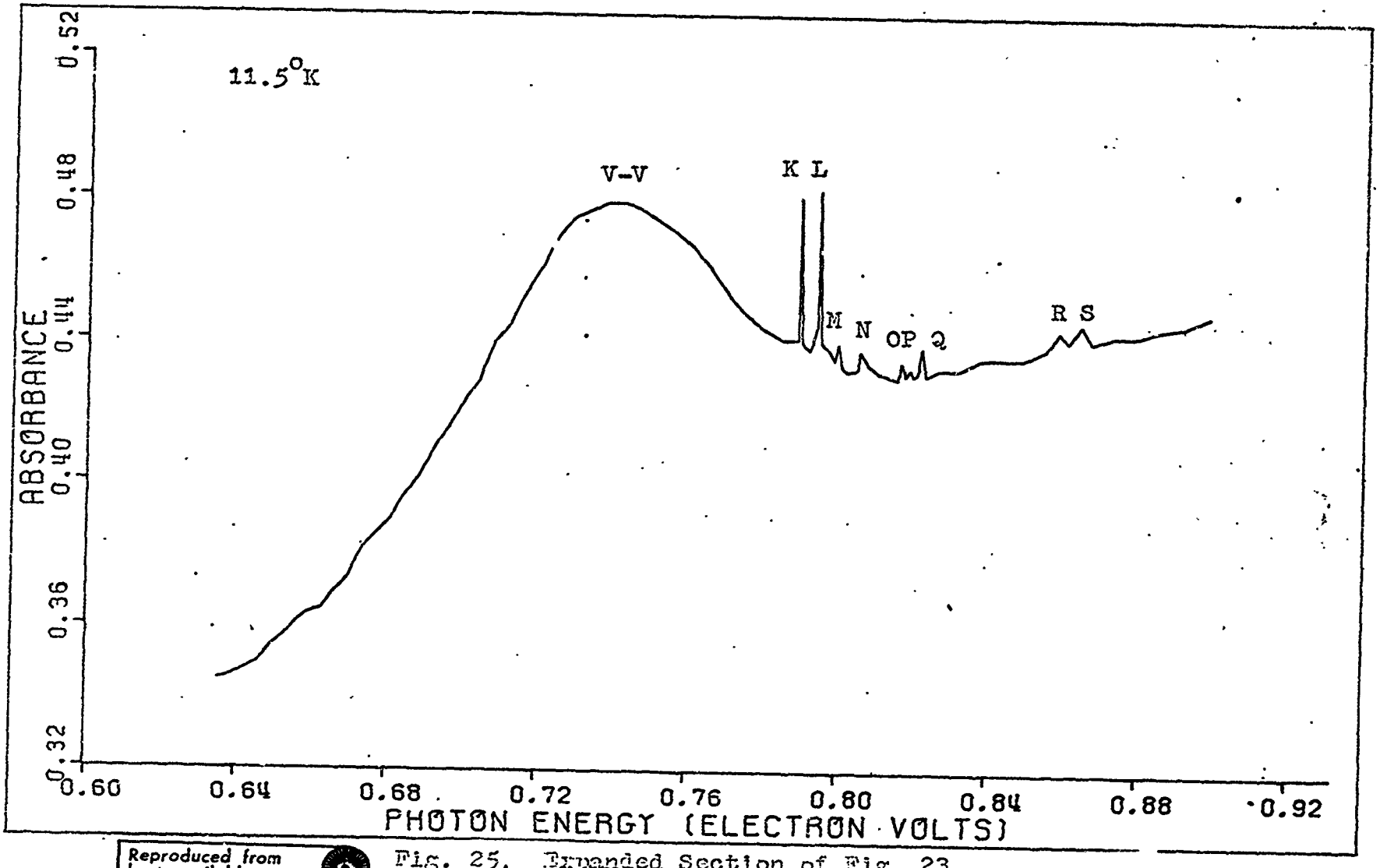

Fig. 25. Expanded Section of Fig. 23
Energy range 0.64 eV to 0.91 eV

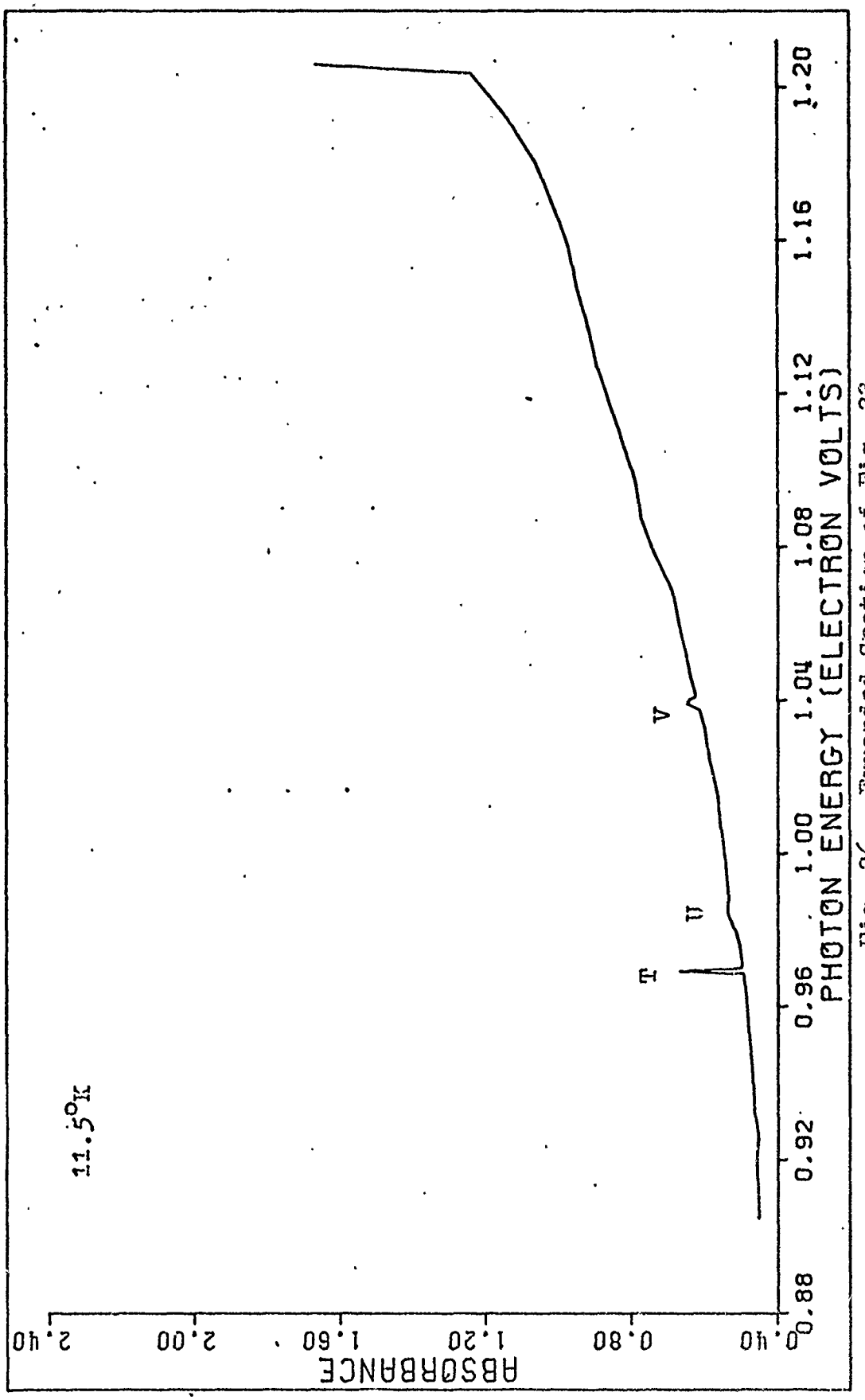

Fig. 26. Expanded Section of Fig. 23
Energy range 0.90 eV to 1.20 eV

Table V

Absorption Bands at Liquid Helium Temperature

Note: OBW-observed band width
SBW-spectral band width(instrumental resolution)
NBW-natural band width
Columns left blank indicate peak was too small to accurately measure band width

Band	Wavelength (micron)	Energy (eV)	OBW (Å)	SBW (Å)	NBW (Å)	NBW (meV)
A	2.535	0.4891	20.8	16.6	12.5	0.24
B	2.459	0.5042	370	10.1	370	7.58
D	2.404	0.5158				
F	2.371	0.5229	17.3	9.0	14.8	0.33
H	2.238	0.5540	38	7.3	37.3	0.93
V-V	1.682	0.7372	1620	5.6	1620	71.0
K	1.570	0.7898	7.7	3.8	6.7	0.34
L	1.560	0.7948	11.3	3.8	10.6	0.54
M	1.549	0.8005				
N	1.539	0.8057				
O	1.518	0.8168				
P	1.514	0.8190				
Q	1.509	0.8217				
R	1.443	0.8593				
S	1.432	0.8659				
T	1.278	0.9702	5.9	3.0	5.1	0.30
U	1.261	0.9833	79	3.4	79	6.16
V	1.192	1.0402	9.4	3.7	8.6	0.75

was chosen for, from previous luminescence studies, only the 0.970 eV zero-phonon line and phonon-assisted sideband structure was seen in irradiated float zone crystals (Ref 20,22,33,41). Sample Z was irradiated to a fluence of $4x10^{18}$ e/cm^2 and again to a total fluence of $6x10^{18}$ e/cm^2. However, in each case, no radiation damage was observed. Sample O, a pulled silicon crystal, was cut to a thickness of 1.69 mm to confirm that a thinner sample than A(5.74 mm) could be used. Sample O was irradiated to a fluence of $4x10^{18}$ e/cm^2. The recorded spectrum contained the same defect structure as that recorded for sample A, but with not as great detail for the sideband structure.

Another float zone crystal, sample X, was cut to a thickness of 1.89 mm and irradiated to a fluence of $2x10^{18}$ e/cm^2. Only a narrow band of very small intensity was observed at 0.9695 eV. The sample was irradiated to a total fluence of $4x10^{18}$ e/cm^2, the same fluence to which sample O had been irradiated, in order to compare the intensity of the narrow band at 0.9695 eV. The intensity of the band was down by a factor of 7 in sample X compared to that in sample O.

Comparison of Absorption and Luminescence Spectra

The second stated purpose of this study was to compare the absorption spectra obtained from irradiated silicon samples with that obtained by recombination luminescence for irradiated silicon samples of the same type. This comparison is made in two ways. First, the structure of the spectra

are compared by including both absorption and luminescence spectra on one figure. Bands labeled with a different notation than that of the original author were done for ease of identification in the comparison. Second, a table, which accompanies each figure, shows the comparison of the energy locations for the zero-phonon lines and the phonon-assisted peaks, in addition to identifying the corresponding peak notations. The column labeled Separation is the energy difference between the phonon-assisted peak and the prominent narrow line.

0.489 eV Line. The comparison of the structure of the absorption spectrum from sample A at 11.5°K with that of the luminescence spectrum at 20.4°K reported by Panin, et al. (Ref 30) is shown in Fig. 27. The energy comparisons are presented in Table VI. The bands chosen for comparison from Panin, et al. were the narrow band at B_o and two of the phonon-assisted peaks, B_1 and B_{15}.

Table VI

0.489 eV Line Comparison

Absorption			Luminescence		
Band	Energy (eV)	Separation (meV) X-A	Band	Energy (eV)	Separation (meV) X-B_o
A	0.4891		B_o	0.490	
B	0.5042	15.1	B_1	0.478	12
D	0.5158	26.7	B_2	0.471	19
F	0.5229	33.8	B_{15}	0.456	34

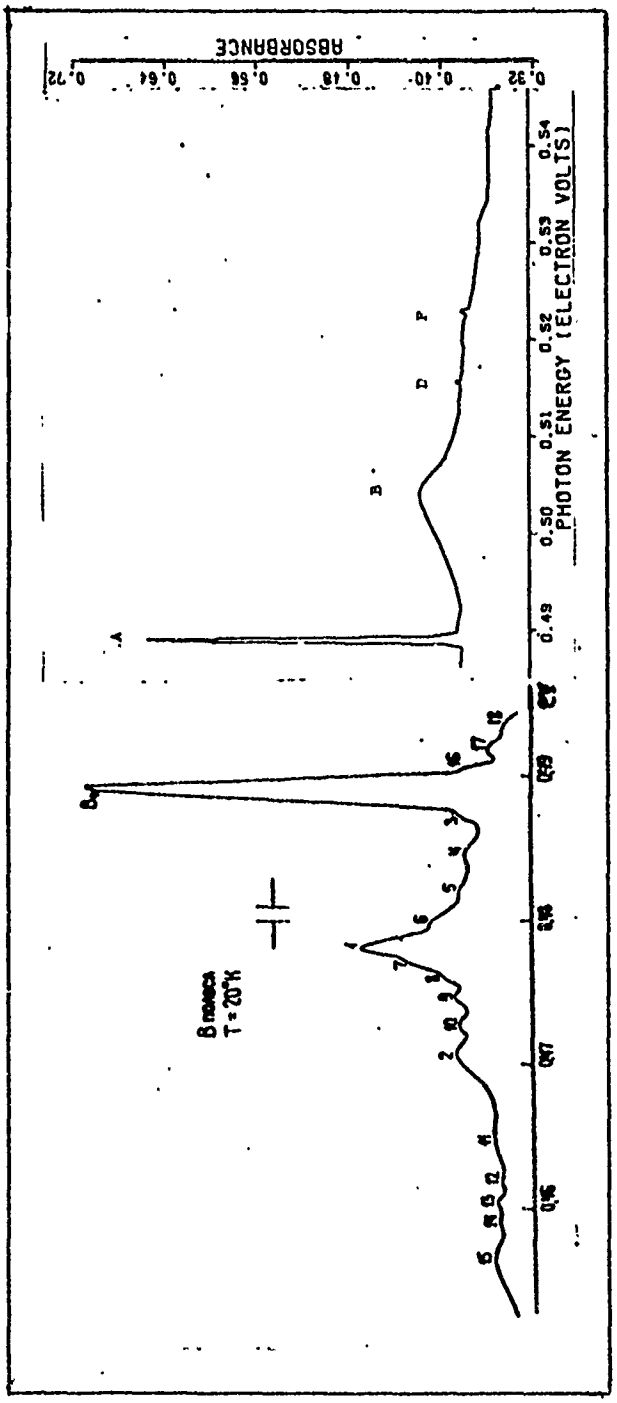

Fig. 27. Absorption-Luminescence Spectra Comparison
0.489 eV Line.

0.790 eV and 0.795 eV Lines. The comparison of the absorption and luminescence spectra from pulled samples containing these zero-phonon lines is shown in Fig. 28. The luminescence spectra reported by Jones and Compton (Ref 22:84) was recorded at 34°K. The energy comparison is presented in Table VII. Phonon-assisted peaks 1 and 2 were labeled for ease of identification. Since the sharp lines at 0.7898 eV (K) and 0.7948 eV (L) occurred in equal intensity as did the phonon-assisted sideband pairs, the energy separation was calculated between the sharp line and its corresponding phonon-assisted peak. For the luminescence spectrum, since the zero-phonon line at 0.790 eV (C) was the most intense, the energy separation is calculated from this line for the phonon-assisted peaks.

Table VII

0.790 eV and 0.795 eV Line Comparison

Absorption				Luminescence		
Band	Energy (eV)	Separation (meV) X-K	X-L	Band	Energy (eV)	Separation from C (meV)
K	0.7898			C	0.790	
L	0.7948	5		D	0.795	5
M	0.8005	10.7		1	0.772	18
N	0.8057		10.9			
O	0.8168	27		2	0.744	26
Q	0.8217		26.9			
R	0.8593	69.5		A	0.717	73
S	0.8659		71.1			

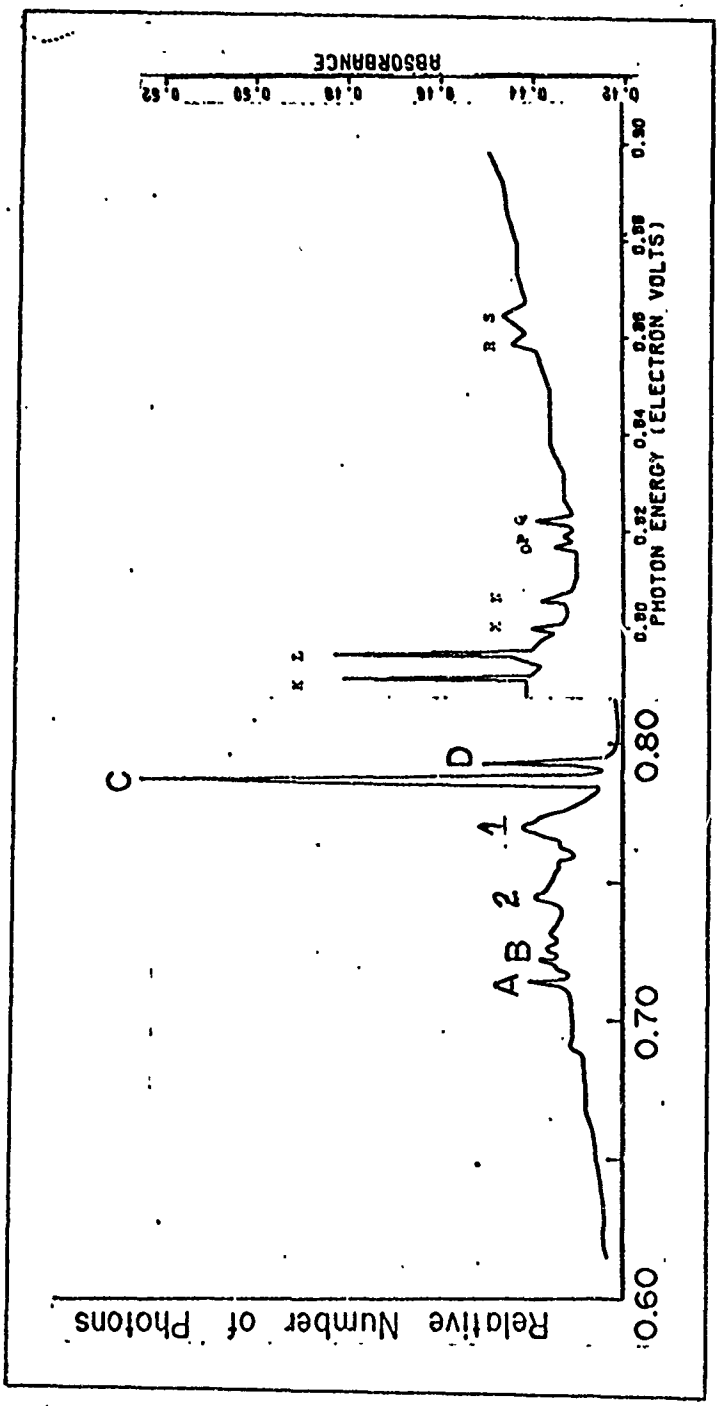

Fig. 28. Absorption-Luminescence Spectra Comparison
0.790 eV and 0.797 eV lines

0.970 eV Line. The comparison of the absorption and luminescence spectra from pulled samples containing this zero-phonon line is shown in Fig. 29. The luminescence spectra reported by Jones and Compton (Ref 22) was recorded at 34°K. The energy comparison is presented in Table VIII. Phonon-assisted peak 3 was labeled for ease of identification.

Table VIII

0.970 eV Line Comparison

Absorption			Luminescence		
Band	Energy (eV)	Separation (meV) X-T	Band	Energy (eV)	Separation (meV) X-G
T	.9702		G	0.970	
U	.9833	13.1	3	0.955	15
V	1.0402	70.0	E	0.898	72

Table IX shows the energy comparison between the results from sample A and a luminescence spectrum, recorded at liquid helium temperature, of a sample cut from the same boule as used in this study. The luminescence spectrum was recorded by Dr. R. J. Spry of the Air Force Materials Laboratories. The sample was irradiated to a fluence of 1×10^{17} e/cm^2 with 0.73 MeV electrons from a Van de Graaff generator.

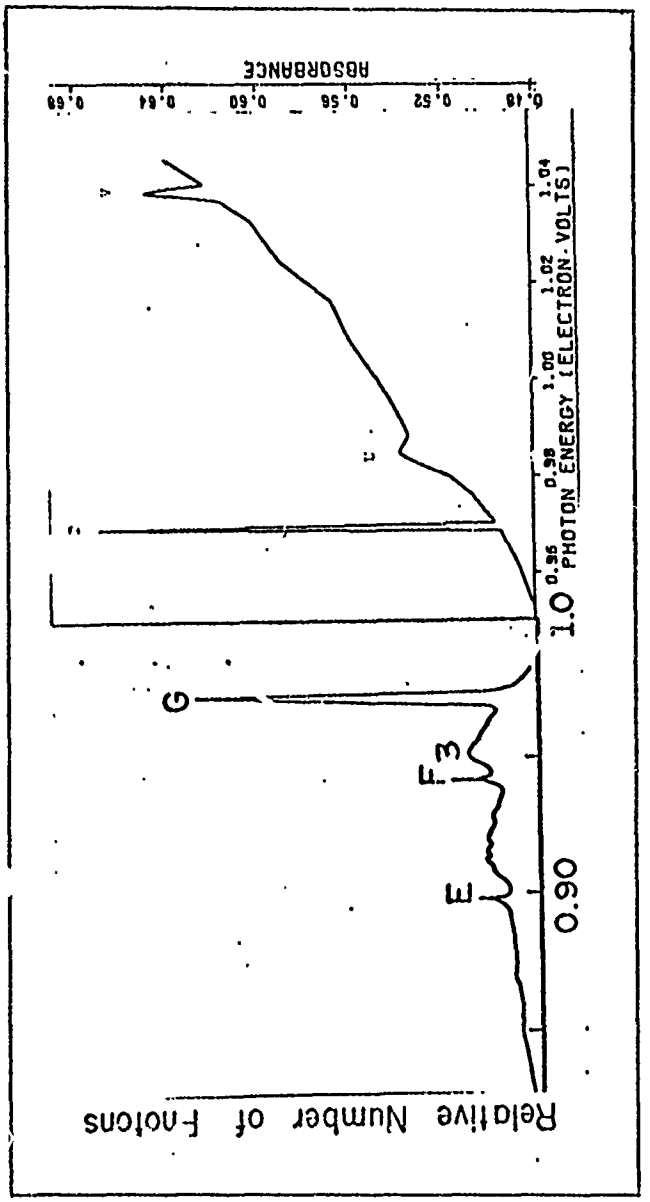

Fig. 29. Absorption-Luminescence Spectra Comparison
0.970 eV Line.

Table IX

Absorption and Luminescence from Same Silicon Boule

Absorption		Luminescence
Band	Energy (eV)	Energy (eV)
A	0.4891	0.4886
K	0.7898	0.7902
L	0.7948	0.7945
T	0.9702	0.9692

Dose Rate Study

The purpose of the dose rate study was to determine which phonon-assisted lines could be related to the sharp lines and also if there was a relationship between any of the sharp lines. An initial interpretation of the spectra shown in Figs. 23 thru 26 and the peak locations presented in Table V is that there are three sets of sharp lines and phonon-assisted sideband structures which are related. However, this picture is only true for one irradiation value. The growth rate of these lines was therefore studied as a function of the fluence. For this study, sample E, a pulled silicon crystal was used. The sample was subjected to total fluences of 0.5, 1, 2, 5, and 7.6×10^{18} e/cm^2. The following figures show the growth rate of the sharp lines and the major phonon-assisted peaks observed in the spectra. The intensity value is the height in mm of the respective sharp line or phonon-assisted peak.

The growth rate of lines A, B, and H is shown in Fig.30 . These lines did not appear until a fluence of $2x10^{18}$ e/cm^2. At a fluence of $7.6x10^{18}$ e/cm^2 the lines were no longer observed. Fig.31 shows the growth rate of lines T, U, and V. The band at U did not appear until a fluence of $1x10^{18}$ e/cm^2. This was a broad band and at such a small radiation dose as $5x10^{17}$ e/cm^2 the line could not be separated from the background. All lines except T disappeared at a fluence of $7.6x10^{18}$ e/cm^2. Line T did not disappear completely but was drastically reduced. The growth of lines K and L is plotted in Fig.32 . These were the only lines which did not decrease at a fluence of $7.6x10^{18}$ e/cm^2. The growth of the major lines A, T, and K was plotted along with the divacancy (V-V). As shown in Fig.33 , the intensity of the divancy was reduced at $7.6x10^{18}$ e/cm^2.

To check that the disappearance of most of the lines at a fluence of $7.6x10^{18}$ e/cm^2 was not caused by annealing during irradiation or an experimental error, another pulled silicon sample was irradiated. This crystal, sample H, was irradiated to a fluence of $5x10^{18}$ e/cm^2. The intensities of all the lines were found to be at approximately the same value as those of sample E at $5x10^{18}$ e/cm^2. Sample H was then irradiated to a total fluence of $7.6x10^{18}$ e/cm^2. Again the only lines which remained at their same intensity were K and L as is seen in Fig.34 . The divacancy was again reduced but still present. The loss of intensity due to a high fluence value was also noted by Johnson (Ref 19:76) and

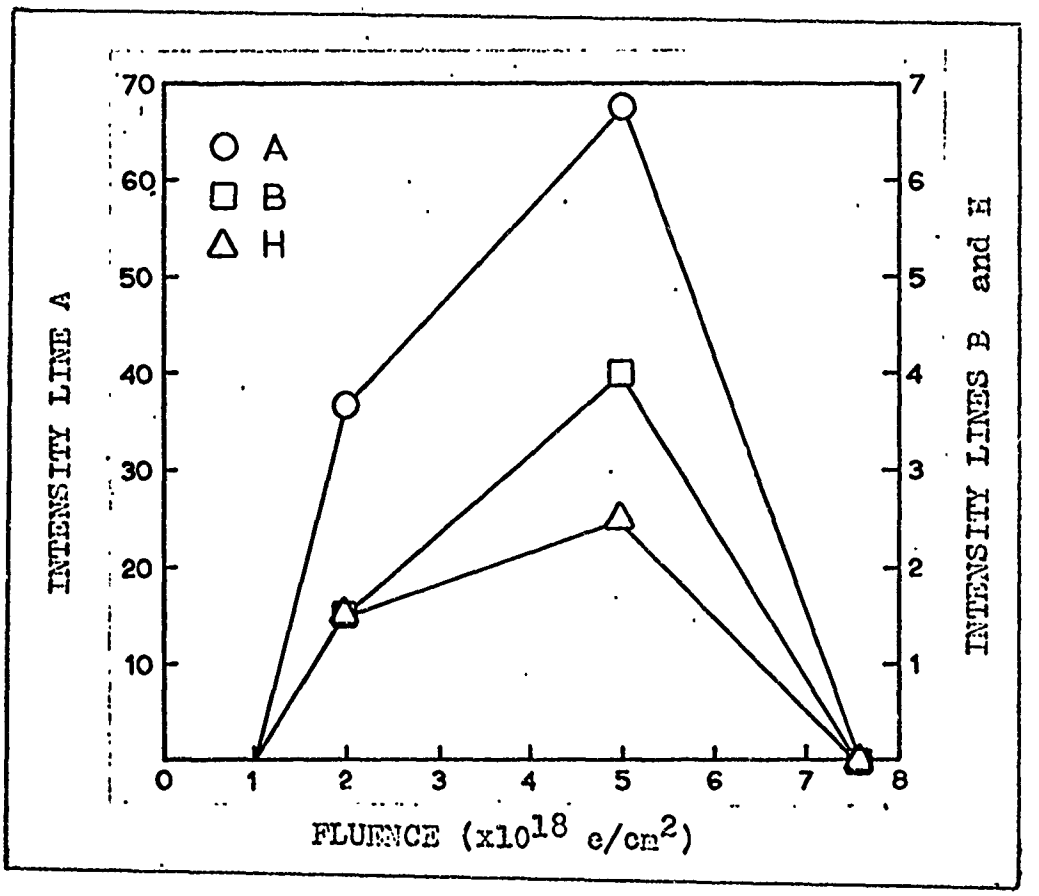

Fig. 30. Growth Rate of Lines A,B, and H

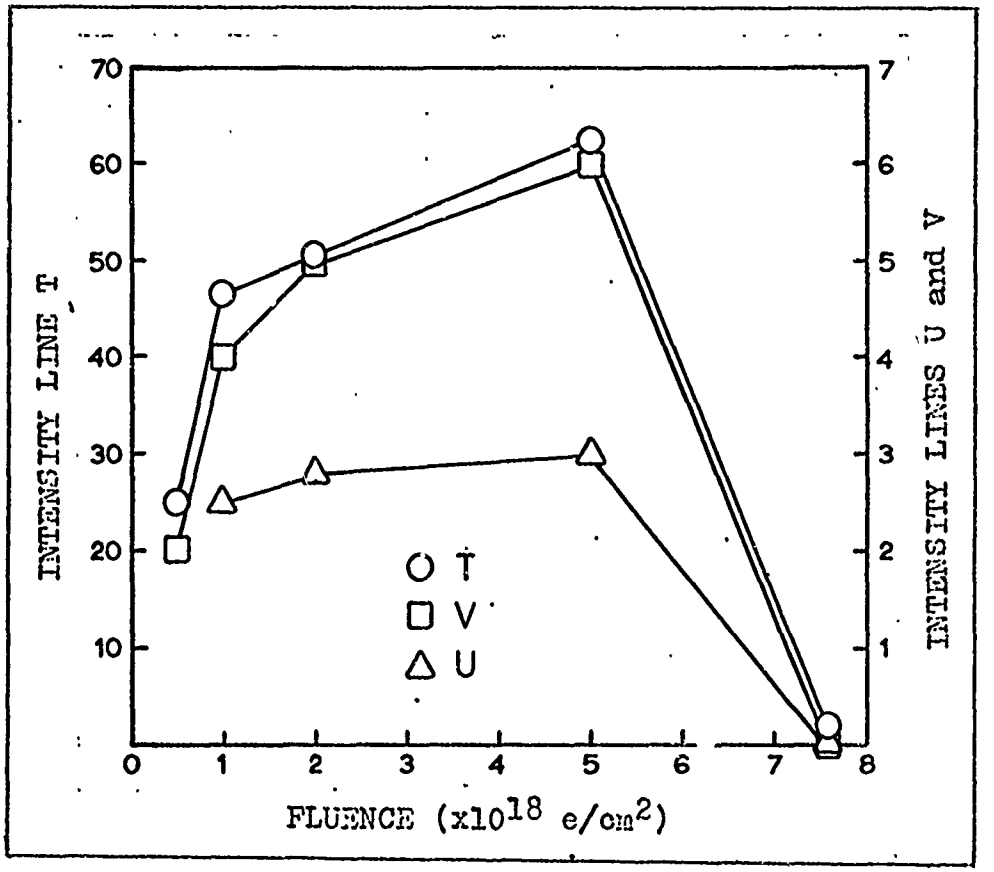

Fig. 31. Growth Rate of Lines T,U, and V

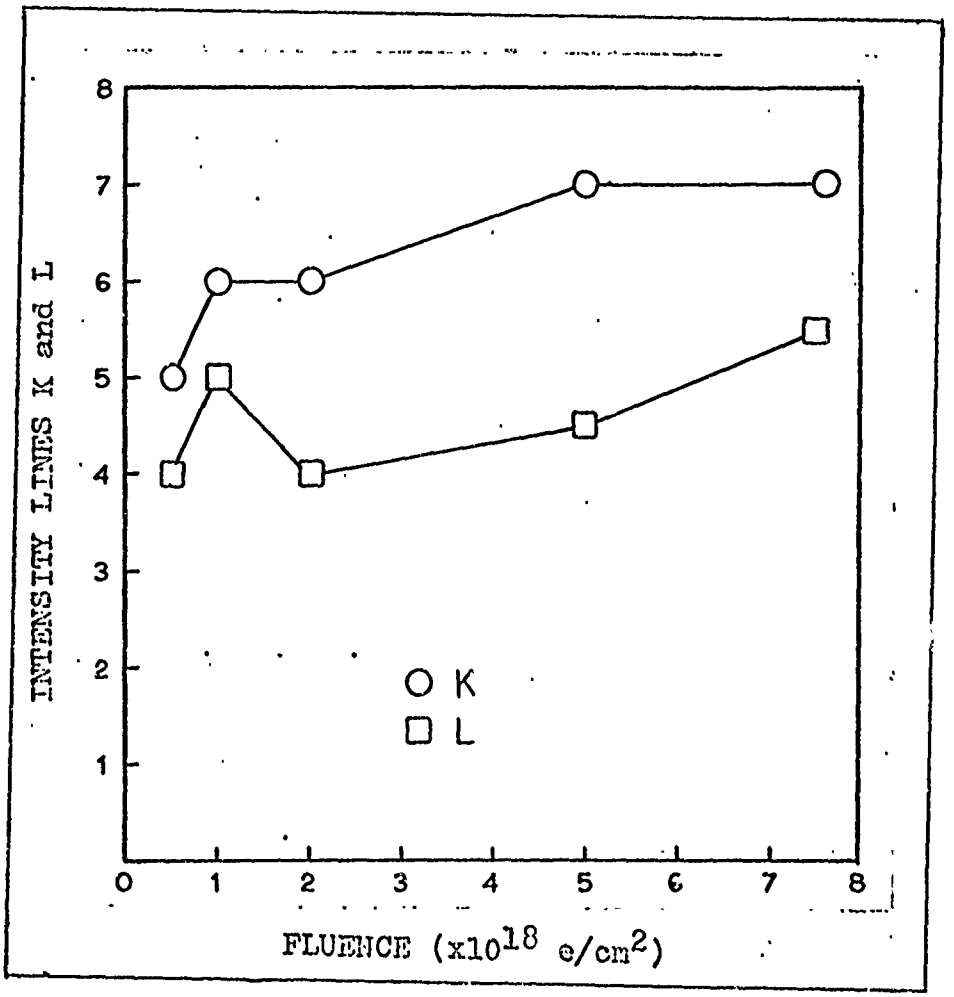

Fig. 32. Growth Rate of Lines K, and L

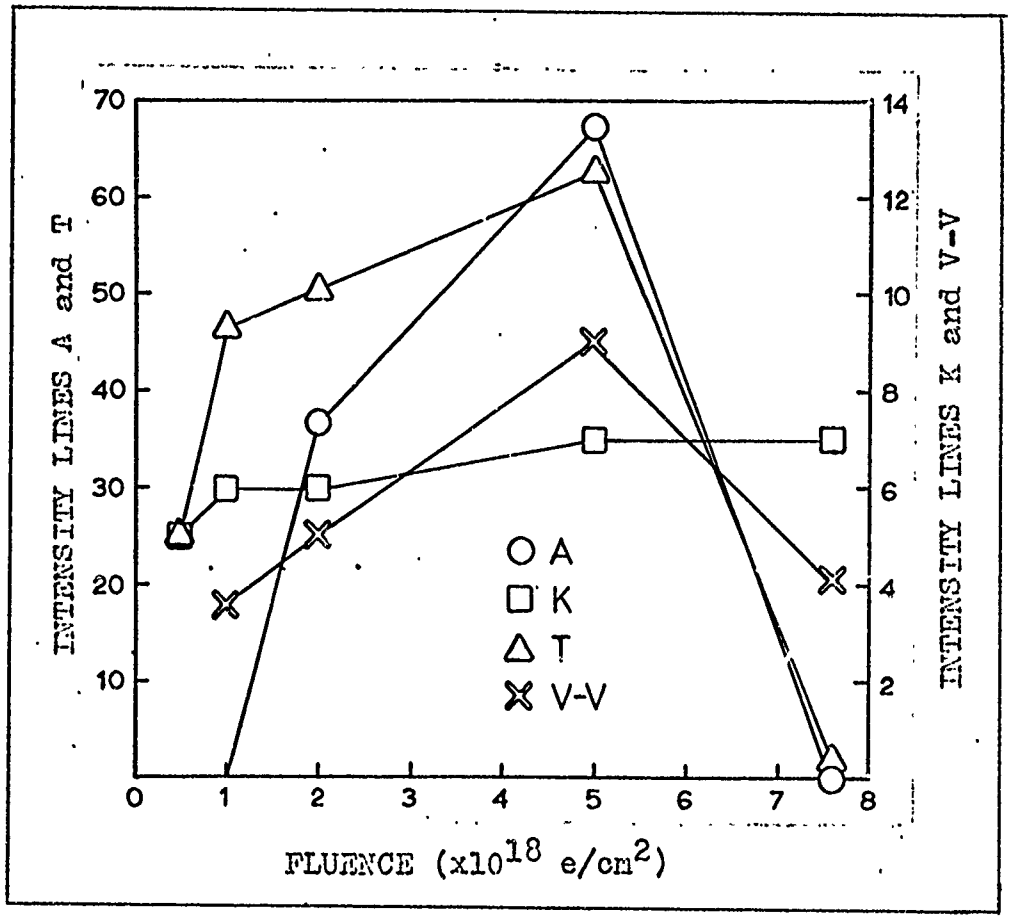

Fig. 33. Growth Rate of Lines A,K,T, and V-V Sample E.

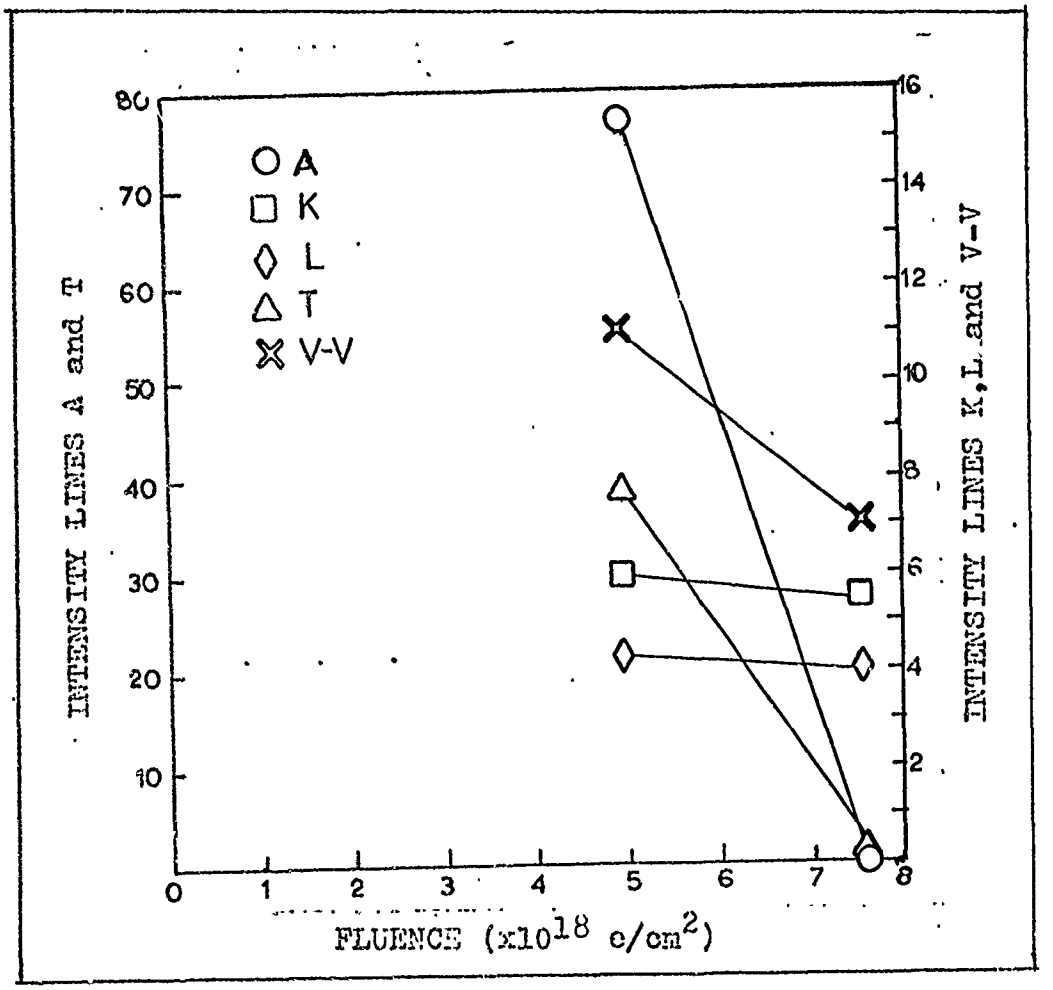

Fig. 34. Growth Rate of Lines A,K,L, T and V-V Sample H.

Panin, et al. (Ref 30).

Bean, et al. measured the growth rate of bands b (1.69 microns) and c (2.54 microns) as a function of irradiation dose. These bands correspond to band V-V (1.682 microns) and the sharp line at A (2.535 microns) in this study. A comparison of the two growth rate studies is shown in Fig. 35.

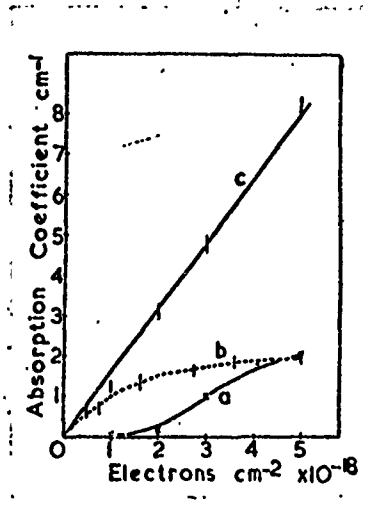

Curves b and c are for divacancy. Curve a is 2.54 micron band. Solid curve for high Carbon content; dashed curve for low Carbon content (Ref 4).

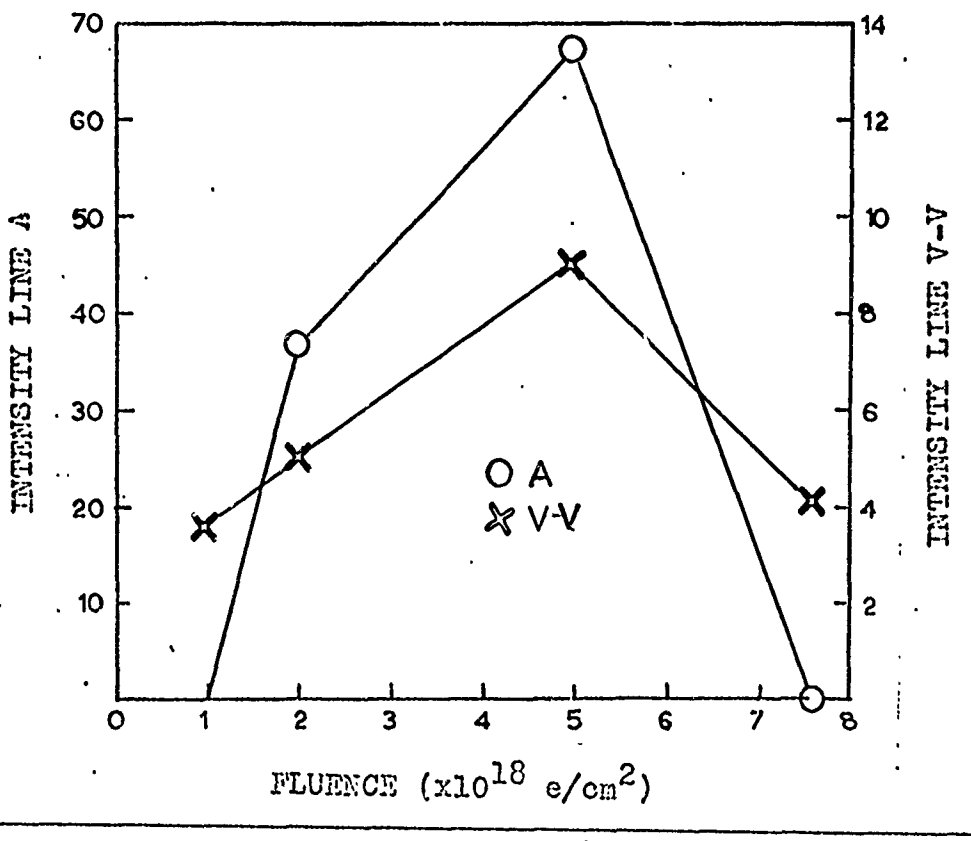

Fig. 35. Comparison of Growth Rate Studies Sample E vs. Bean, et al. study.

VII Discussion and Conclusions

The first section of this chapter contains a discussion of the experimental results. Included are the comparisons made with luminescence spectra and the identification of the sharp lines, a tentative assignment of the phonons emitted, and the results of the dose rate study. The final section presents the conclusions of this project and recommendations for further study.

Discussion

Zero phonon lines are identified as such by their extreme narrowness and usually proved to be such by observation of an emission and absorption line at the same frequency (Ref 34:242). The values of kT at 79°K and 11.5°K are 6.8 meV and 0.99 meV, respectively. As seen in Table III and V the natural band widths of the sharp lines at 0.4891 eV (A), 0.7898 eV(K), 0.7948 eV (L), and 0.9702 eV (T) are all very much less than kT at both 79°K and 11.5°K. This indicates that these lines are probably all due to the creation of excitons bound at defect centers. However, the type of centers involved (charged, neutral, etc.) cannot be determined from the band width analysis. The energies at which each of these four lines, A, K, L, and T, occur in the absorption spectra of this study correspond to the energies of zero-phonon lines identified in luminescence spectra. Table VI, VII, and V :I list these comparisons for the known zero-phonon locations as well as Table I. Striking evidence

of the observation of an emission and absorption line at the same frequency is given in Table IX. These four sharp lines were seen for samples cut from the same single crystal silicon boule in both the absorption and luminescence spectra. This evidence indicates the sharp lines at A, K, L, and T seen at both liquid nitrogen and liquid helium temperature in the absorption spectra are zero-phonon lines.

The comparison of the absorption and luminescence spectra shown in Figs. 27, 28, and 29 indicate that the phonon-assisted structure is reflected around the zero-phonon lines in the absorption spectra. Although the absorption and luminescence spectra do not exhibit complete mirror symmetry, there are 7 phonon-assisted peaks which correspond in both types of spectra and are mirrored about the zero-phonon lines. These are the absorption peaks at B, F, U, and V, and the three pairs M, O, and R or N, Q, and S. The comparisons are listed in Table VI, VII, and VIII.

The zero-phonon lines at 0.7898 eV (K) and 0.7948 eV (L) occurred at equal intensities in the absorption spectra recorded at both liquid nitrogen and liquid helium temperatures as seen in Figs. 21 and 25. Jones (Ref 21) observed that the intensities of the zero-phonon lines at 0.790 eV (C) and 0.795 eV (D) in Fig. 9 occurred at different intensities when the temperature at which the luminescence spectra were recorded varied. Jones' conclusion that the splitting of the energy level in the excited state is confirmed by the findings in the absorption spectra of this study.

If the splitting had been in the ground state energy level, the absorption spectra would have shown the intensity changes with variation in temperature. The energy level splitting and transitions involved are shown in a simple schematic in Fig. 36. The initial states for both the absorption and luminescence process are those levels from which the transition arrows originate. It must be assumed that in each process there is an equal probability for the two transitions, A and B.

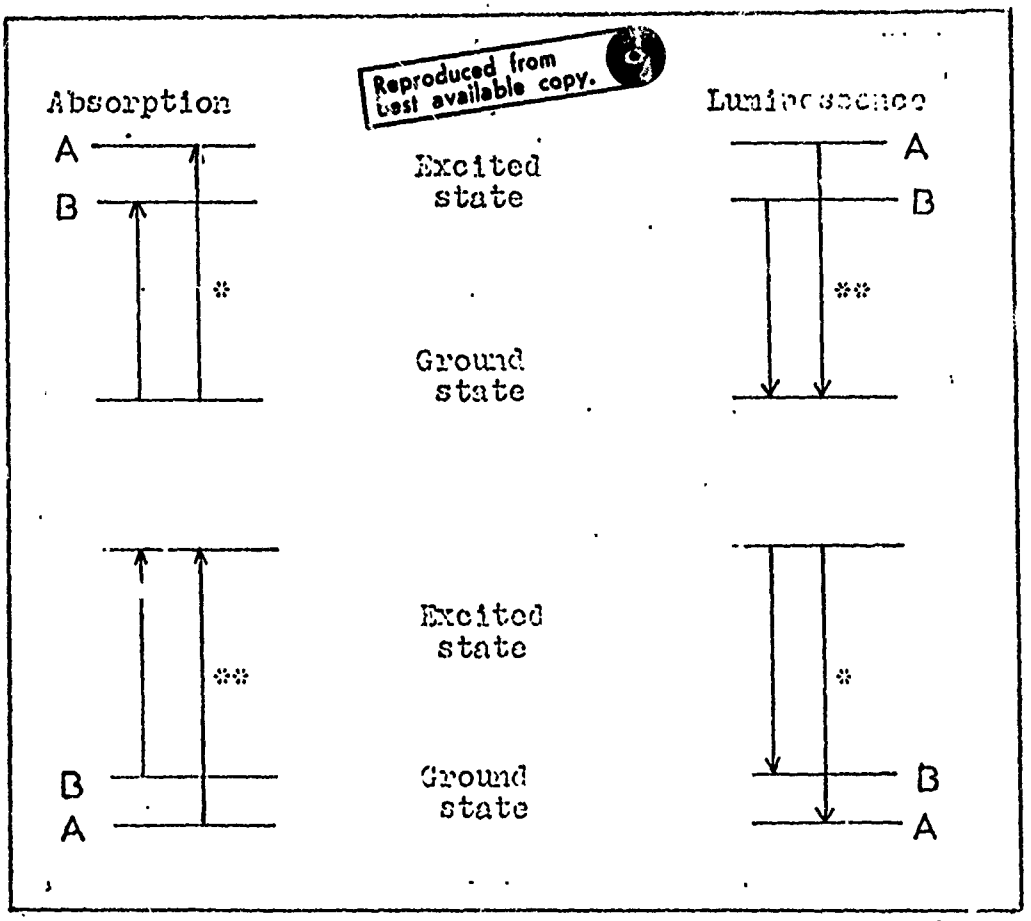

Fig. 36. Comparison of Absorption and Luminescence Process.
Level A corresponds to 0.795 eV transition.
Level B corresponds to 0.790 eV transition.
* indicates equal intensity of lines.
** indicates intensity of lines related by a Boltzmann factor.

For two temperatures, the initial state of the transition process must be equally populated to result in equal intensities of these two lines. If the ground state energy level were split then the luminescence spectra would exhibit these two lines in equal intensities since the initial state (excited state) of luminescence process would be equally populated.

Fig. 30 shows the relationship between the zero-phonon line at A and its associated phonon-assisted side band structure. It can be seen that the small phonon-assisted peaks at B and H are related to the zero-phonon line at A. Fig. 31 exhibits the same type of relationship between the zero-phonon line at T and the phonon-assisted peaks at U and V. Zero-phonon lines at K and L are related as is shown in Fig. 32. The growth rate of the phonon-assisted sideband structure for these zero-phonon lines was not plotted since the intensities of those peaks were relatively small. However, the phonon-assisted peaks also appeared in pairs during, the dose rate study. Thus the energy separations between the zero-phonon lines and associated phonon-assisted peaks in Table VII are consistent with the results seen during the dose rate study.

A tentative assignment of the phonons emitted is presented in Table X.

Table X

Phonon Assignment

Note: LM-local mode
TA-transverse acoustic
ZC-zone center optical
Separation is energy difference between phonon-assisted peak and zero-phonon line.

Band	Energy (eV)	Separation (meV)	Phonon emitted
A	.4891		Zero
B	.5042	15.1	TA
D	.5158	26.7	?
F	.5229	33.8	2TA
H	.5540	64.9	ZC or LM
K	.7898		Zero
M	.8005	10.7	TA
O	.8168	27	?
R	.8593	69.5	LM
L	.7948		Zero
N	.8057	10.9	TA
Q	.8217	26.9	?
S	.8659	71.1	LM
T	.9702		Zero
U	.9833	13.1	TA
V	1.0402	70.0	LM

According to Thomas (Ref 34:250), the local mode sidebands are very sharp. Since the peaks at H and V are very sharp, they are probably due to local modes instead of zone center optical phonons. There appears to be a similar pattern of the emitted phonons for the sharp lines at A, K, and L. The pattern consists of a TA phonon, a phonon with an energy of 27 meV of unknown origin, and a zone center optical phonon or local mode vibration. The pattern for the line at T is similar except there is no 27 meV phonon emitted.

The growth rate of the zero-phonon lines at A, K, and T are plotted along with that of the divacancy (V-V) in an attempt to relate any of these prominent lines. There seems to be no relation between any of these lines, as seen in Fig. 33 , and thus the three zero-phonon lines and their associated phonon-assisted sidebands are independent of each other. The lines at 0.7898 eV (K) and 0.9702 eV (T) are independent of the band at V-V and cannot be related to the divacancy.

A comparison of the dose rate studies shown in Fig. 35 indicates that the growth rate of curve a (for 2.54 micron band) reported by Bean, et al. agrees with that of the zero-phonon line at 0.4891 eV (A) in this study. The growth of the line at A may or may not follow the growth of the divacancy (V-V) but the line at A is found only in pulled silicon samples. The divacancy was seen in both pulled and float-zone samples. Thus the line at A may not be associated with the divacancy.

The disappearance or reduction in intensity of all lines except the ones at 0.7898 eV (K) and 0.7948 eV (L) at a fluence of 7.6×10^{18} e/cm^2 was observed on two different samples at the same fluence value. This loss in intensity may be due to the interaction of the defect states or a result of lowering of the Fermi level.

The lines at K and L are found only in pulled samples and are therefore dependent on oxygen for their formation. The energy for the transition corresponds to a ground state

energy level at E_v + 0.37 eV. The assignment of the energy level with respect to the valence band is consistent with the results of the dose rate study. Although the Fermi level was changing for the n-type sample as the electron fluence increased, the intensity of the lines at K and L remained constant at these higher fluence values. This indicates that the ground state is in the lower half of the gap. The dependence on oxygen and the ground state level at E_v + 0.37 eV are in good agreement for identification of the defect with the K center.

If the loss of intensity of the lines at A and T are due to lowering of the Fermi level, the ground state energy levels of the associated defects are probably in the upper half of the gap.

Jones and Compton (Ref 22) reported that the lines at 0.717 eV, 0.722 eV, 0.898 eV, and 0.941 eV were zero-phonon lines. However, these lines were not seen in the absorption spectra of this study. The energy separation of the lines at 0.717 eV and 0.898 eV from the zero phonon lines at 0.790 eV and 0.970 eV did correspond to phonon-assisted peaks listed in the comparisons presented in Tables VII and VIII.

Conclusions

The important result of this study was the detection of sharp lines in the absorption spectra of electron irradiated silicon samples and the important conclusion was the identification of these lines as zero-phonon lines.

Three families of bands were seen. Two of the families consisted of a zero-phonon line with the phonon-assisted sideband structure on the high energy side of the zero-phonon line. The other family consisted of two zero-phonon lines each with its own phonon-assisted sideband structure on the high energy side of the zero-phonon lines.

The four major zero-phonon lines correspond to those previously seen in luminescence spectra and also in the luminescence spectrum of a sample cut from the same silicon boule used in this study.

The families of lines at 0.4891 eV, 0.7898 eV, and 0.7948 eV were seen only in pulled silicon samples while the family at 0.9702 eV was seen in both pulled and float zone silicon samples. This confirmed similar findings in luminescence spectra.

The findings of Jones (Ref 21) that the zero-phonon lines occurring at 0.790 eV and 0.795 eV are due to the splitting in the excited state of the defect's energy level are confirmed. This was shown by the equal intensity of the lines in the absorption spectra.

The results of the dose rate study showed that the three major families of lines are independent of each other. The lines at 0.9702 eV, 0.7898 eV and 0.7948 eV are independent of the broad band (V-V) identified with the divacancy. The family of lines at 0.4891 eV may follow the growth of the divacancy but this is not a definite conclusion.

The intensities of most of the zero-phonon lines and associated phonon-assisted peaks were drastically reduced in two samples which were irradiated to a total fluence of 7.6×10^{18} e/cm^2. Only the lines at 0.7898 eV and 0.7948 eV did not decrease. These two lines were identified with the K center.

It is recommended that more silicon samples containing various impurities be irradiated and the resulting defects examined by absorption spectroscopy. The results should then be compared with luminescence spectra. A dose rate study should be conducted on samples cut from the boules used in this study. A smaller initial fluence should be used along with smaller integral doses. The fluence value at which the majority of the lines disappeared in this study should be approached more slowly. An alternate to this study would be an annealing study of these zero-phonon lines in hopes of identifying the defect centers.

Bibliography

1. Almeleh, N. and B. Goldstein. "Electron Paramagnetic Resonance and Electrical Properties of the Dominant Paramagnetic Defect in Electron Irradiated p-Type Silicon." Physical Review, 149:687-692 (1966).

2. Applied Physics Corporation Instructions For Cary Recording Spectrophotometer Model 14 RI. Monrovia, Calif. Cary Instruments.

3. Baker, J. A., et al. "Effect of Carbon on the Lattice Parameter of Silicon." Journal of Applied Physics, 39:4365-4368 (1968).

4. Bean, A. R., et al. "Electron Irradiation Damage in Silicon Containing Carbon and Oxygen." Journal of the Physics and Chemistry of Solids, 31:739-751 (1970).

5. Bemski, G. "Paramagnetic Resonance in Electron Irradiated Silicon." Journal of Applied Physics, 30:1195-1198 (1959).

6. Bortnik, M. V., et al. "Radiative Recombination of Radiation Defects in Silicon." Soviet Physics-Semiconductors, 1:290-294 (1967).

7. Brockhouse, B. N. "Lattice Vibrations in Silicon and Germanium." Physical Review Letters, 2:256-258 (1959).

8. Cahn, J. H. "Irradiation Damage in Germanium and Silicon to Electrons and Gamma Rays." Journal of Applied Physics, 30:1310-1316 (1959).

9. Cheng, L. J., et al. "1.8-,3.3, and 3.9 μ Bands in Irradiated Silicon: Correlations with the Divacancy." Physical Review, 152:761-774 (1966).

10. Corbett, J. W. Electron Radiation Damage in Semiconductors and Metals. New York: Academic Press, 1966.

11. Corbett, J. W., et al. "Defects in Irradiated Silicon. II. Infrared Absorption of the Si-A Center." Physical Review, 121:1015-1022 (1961).

12. Dean, P. J. "Lattices of the Diamond Type." in Luminescence of Inorganic Solids edited by P. Goldberg. New York: Academic Press (1966).

13. Dean, P. J., et al. "Absorption due to Bound Excitons in Silicon." Physical Review, 163:721-725 (1967).

14. Fan, H. Y. and A. K. Ramias. "Infrared Absorption and Photoconductivity in Irradiated Silicon." Journal of Applied Physics, 30:1127-1134 (1959).

15. Fitchen, D. B. "Zero-Phonon Transitions" in Physics of Color Centers edited by W. B. Fowler. New York: Academic Press, 1968.

16. Haynes, J. R. "Experimental Proof of the Existence of a New Electronic Complex in Silicon." Physical Review Letters, 4:361-363 (1960).

17. Hopfield, J. J. "The Quantum Chemistry of Bound Exciton Complexes." in Physics of Semiconductors. New York: Academic Press, 1964.

18. Hrostowski, H. I. "Infrared Absorption of Semiconductors" in Semiconductors edited by N. B. Hannay. New York: Reinhold 1960.

19. Johnson, E. S. Recombination Luminescence in Irradiated Silicon: Effects of Thermal Annealing and Lithium Impurity. PhD Thesis Report R-502 University of Illinois, 1971.

20. Johnson, E. S. and W. D. Compton. "Recombination Luminescence in Irradiated Silicon-Effects of Thermal Annealing and Lithium Impurity." Radiation Effects, 9:89-92 (1971).

21. Jones, C. E. The Effect of Stress on the Luminescence Spectrum of Irradiated Silicon. PhD Thesis Report R-466 University of Illinois, 1970.

22. Jones, C. E. and W. D. Compton. "Recombination Luminescence in Irradiated Silicon - Effects of Uniaxial Stress and Temperature Variations." Radiation Effects, 9:83-88 (1971).

23. Kaiser, W. and P. H. Keck. "Oxygen Content of Silicon Single Crystals." Journal of Applied Physics, 28:882-887 (1957).

24. Kelly, B. T. Irradiation Damage to Solids. New York: Pergamon Press, 1966.

25. Knox, R. S. Theory of Excitons. New York: Academic Press, 1963.

26. Macfarlane, G. G., et al. "Fine Structure in the Absorption - Edge Spectrum of Si." Physical Review, 111:1245-1254 (1958).

27. Moss, T. S. Optical Properties of Semiconductors London: Butterworth and Co. Limited, 1961.

28. Nelms, A. T. "Energy Loss and Range of Electrons and Positrons." NBS Circular 577, US Dep. of Comm., 1956.

29. Newman, R. C. and R. S. Smith. "Vibrational Absorption of Carbon and Carbon-Oxygen Complexes in Silicon." Journal of the Physics and Chemistry of Solids, 30:1493-1505 (1969).

30. Panin, V. N., et al. "Radiative Recombination in Irradiated Silicon." Pre print Nr. 155 Order of Lenin Physics Institute, Moscow 1971 Original in Russian. Translated by Leon Marekus Foreign Technology Division. WPAFB, Ohio.

31. Seshadri, K. S. and R. N. Jones. The Shapes and Intensities of Infrared Absorption Bands - A Review. N.R.C. No. 7341. Reprinted from Spectrochimica Acta, 19:1013-1085 (1963).

32. Smith, R. A. Semiconductors New York: Cambridge University Press, 1959.

33. Spry, R. J. and W. D. Compton." Recombination Luminescence in Irradiated Silicon." Physical Review, 175: 1010-1020 (1968).

34. Thomas, D. G. "An Account of Bound Excitons in Semiconductors." in Localized Excitations in Solids, edited by R. F. Wallis. New York: Plenum Press, 1968.

35. Vavilov, V. S. Effects of Radiation on Semiconductors New York: Consultants Bureau, 1965.

36. Watkins, G. D. "EPR and Optical Absorption Studies in Irradiated Semiconductors." in Radiation Effects in Semiconductors, edited by F. L. Vook. New York: Phenum Press, 1968.

37. Watkins, G. D. and J. W. Corbett. "Defects in Irradiated Silicon: Electron Paramagnetic Resonance and Electron-Nuclear Double Resonance of the Si-E Center." Physical Review, 134:A1359-A1377 (1964).

38. Watkins, G. D., et al. "Defects in Irradiated Silicon. I. Electron Spin Resonance of the Si-A Center." Physical Review, 121: 1001-1014 (1961).

39. Wright, D. R., et al. "Luminescence From Natural and Man-Made Diamond in the Near Infrared." Journal of Luminescence, 4:169-193 (1971).

40. Yukhnevich, A. V. "The Structure of the Spectrum of the Radiation Capture of Holes by A-Centers in Silicon." Soviet Physics - Solid State, 7:259-260 (1965).

41. Yukhnevich, A. V. and V. D. Tkachev. "Optical Analog of the Mössbauer Effect in Silicon." Soviet Physics - Solid State, 8:1004-1005 (1966).

VITA

Kennedy Boyd Wilson was born 2 December 1940 in Lancaster, Pennsylvania, the son of Edward G. and Maribelle W. Wilson. He attended Manheim Township High School from which he graduated in 1958. He then attended Gettysburg College at Gettysburg, Pennsylvania, obtaining a Bachelor of Arts degree in Chemistry in June of 1963. After attending officer training school, he received a commission in December of 1963. Capt. Wilson's first two assignments were with the Strategic Air Command as a Missile Launch Control Officer at Lincoln AFB, Nebraska and Malmstrom AFB, Montana. While at Malmstrom AFB he was enrolled in the Minuteman Education Program (AFIT) and a member of the Wing Senior Standardization Crew. Capt. Wilson was assigned to the Air Force Institute of Technology in June of 1970.

Permanent address: 859 Grandview Boulevard
Lancaster, Pennsylvania

This thesis was typed by Mrs. Kathy E. Wilson